A role for the postsynaptic scaffold protein ProSAP1/Shank2 in synaptic maturation

Dissertation zur Erlangung des akademischen Grades des

Doktors der Naturwissenschaften (Dr. rer. nat.)

eingereicht im Fachbereich Biologie, Chemie, Pharmazie der Freien Universität Berlin

vorgelegt von

Stephanie Wegener

aus Magdeburg

2013

This thesis was completed under the supervision of Prof. Dr. Dietmar Schmitz from November 2008 to December 2012 at the Neuroscience Research Center (NWFZ) of the Charité Universitätsklinikum Berlin, Germany.

I hereby declare that the work presented in this thesis has been conducted independently and without inappropriate support. All sources of information are referenced. I hereby declare that this thesis has not been submitted, either in the same or a different form, to this or any other university for a degree.

1st reviewer: Prof. Dr. Stephan Sigrist

2nd reviewer: Prof. Dr. Dietmar Schmitz

Date of Disputation: 3 May 2013

Table of contents

Synopsis

Shanks (also known as ProSAPs/Shanks) are large multidomain proteins that localize to excitatory synapses in the mammalian brain, where they are believed to organize the protein scaffold of the postsynaptic density (PSD). Structurally, Shanks are coupling glutamate receptor scaffolds to the actin cytoskeleton and intracellular signalling pathways by means of their protein-protein interaction domains. Functional studies suggest that Shanks may be important scaffold molecules with a crucial role in the assembly of the PSD during synaptogenesis, in the structural instruction of synaptic plasticity, and in the regulation of dendritic spine morphology. Mutations in all three human *SHANK* genes have been directly linked to patients diagnosed with autism and/or cognitive disability. *Shank2* deficient mice have recently been generated by the laboratory of Prof. Dr. Tobias Böckers (Ulm University, Germany) and we electrophysiologically characterized neuronal transmission of these mice in the CA1 region of the hippocampus. Performing extracellular recordings of evoked field potentials and intracellular whole-cell patch-clamp recordings of spontaneous synaptic transmission, we found that *Shank2*$^{-/-}$ mice suffer from a selective decrease of excitatory synaptic transmission in hippocampal CA1. Recordings of AMPA/NMDA receptor ratios and minimal stimulation experiments revealed that *Shank2*$^{-/-}$ mice suffer from attenuated synaptic maturation, a phenotype that becomes manifest over the course of the fourth postnatal week. Specifically, we found that CA1 pyramidal cells in adolescent (P21-P28), but not juvenile (P13-P14) *Shank2*$^{-/-}$ mice harbour an unusually high fraction of silent synapses. Those synapses that contain AMPA receptors, have a reduced potency. Knockout mice are, however, capable of long-term plasticity as they showed normal long-term depression and increased long-term potentiation. These results confirm a role for Shank2 in the development of excitatory synapses. The late onset of the phenotype in *Shank2*$^{-/-}$ mice, however, questions the hypothesis that Shank2 and Shank3, in contrast to Shank1, are predominantly acting in early synaptogenesis.

Zusammenfassung

Shank Proteine (auch bekannt als ProSAP/Shank Proteine) sind Bestandteile von exzitatorischen Synapsen im Gehirn von Säugetieren und dort vor allem in den postsynaptischen Spezialisierungen (den Dornfortsätzen, englisch: spines) zu finden. Shanks sind große Proteine, die mit Hilfe ihrer unterschiedlichen Protein-Interaktions-Domänen am strukturellen Aufbau der Postsynapse mitwirken. Als Bestandteil der PSD (postsynaptischen Verdichtung) verschränken sie die Ankerproteine der Glutamatrezeptoren mit dem Aktinzytoskelett und intrazellulären Signalkaskaden. Funktionelle Untersuchungen legen nahe, dass Shank Proteine für den Aufbau der PSD während der Synapsenentstehung wichtig sind, aber auch für strukturelle Veränderungen der Postsynapse im Zuge synaptischer Plastizität. Zudem sind für jedes der drei humanen *SHANK* Gene Mutationen beschrieben, die selektiv in Patienten mit Autismus und/oder kognitiven Funktionsstörungen zu finden sind. Um mehr über die Funktion von Shank2 (einem von drei Shank Proteinen in Säugetieren) zu erfahren, wurden von der Arbeitsgruppe um Prof. Dr. Tobias Böckers (Universität Ulm, Deutschland) Shank2 Nullmutanten generiert. Wir haben diese transgenen Mäuse funktionell untersucht, indem wir elektrophysiologische Messungen in der CA1 Region des Hippokampus durchführten. Evozierte, extrazellulär abgeleitete Feldpotentiale sowie intrazellulär gemessene synaptische Spontanaktivität zeigten, dass Shank2 Nullmutanten Störungen speziell der exzitatorischen synaptischen Transmission aufweisen. Messungen der Ratio von synaptischen AMPA- zu NMDA-Rezeptorströmen und Experimente mit Minimalstimulation ergaben darüber hinaus, dass die Synapsen von Shank2 Nullmutanten weniger stark maturiert sind, als dies im Wildtyp der Fall ist. Dieser Phänotyp der Nullmutanten entwickelt sich im Laufe der vierten postnatalen Woche, sodass CA1 Prinzipalzellen von adoleszenten (P21-P28), jedoch nicht von juvenilen (P13-P14) Shank2 Nullmutanten einen höheren Anteil von Synapsen aufweisen, die keine AMPA-Rezeptoren besitzen. Zudem sind die AMPA-Rezeptor vermittelten Ströme in den Shank2 Nullmutanten reduziert. Die Synapsen der Nullmutanten sind jedoch plastisch; so zeigen die Tiere normale synaptische Langzeit-Depression sowie erhöhte synaptische Langzeit-Potenzierung. Der hier beschriebene Entwicklungsphänotyp der Shank2 Nullmutanten belegt die funktionelle Bedeutung von Shank2 für die Entwicklung exzitatorischer Synapsen. Zugleich stellen unsere Ergebnisse die Hypothese in Frage, Shank2 und Shank3 seien - im Gegensatz zu Shank1 - vor allem in frühen Phasen der Synaptogenese wichtig.

1 Introduction

1.1 Synapses are sites of neuronal communication

Neurons are highly specialized cells that receive, integrate, and propagate information to allow for signal processing in the brain. To this end, neurons are equipped with a large number of highly complex contact sites: chemical synapses. Synapses may be formed wherever two neurons come in close enough contact to one another (although synapses can also be formed between a neuron and other cell types). Typically, a neuron's axon gives rise to the presynaptic bouton, and another neuron's dendrite forms the postsynaptic specialization.

Transmission across chemical synapses is mediated primarily by amino acid neurotransmitters, with glutamate being the main excitatory neurotransmitter and γ-aminobutyric acid (GABA) the main inhibitory one in the mammalian central nervous system. The transmitted information is processed by receptors and signalling molecules that are clustered via specialized intracellular protein matrices (for review see Craven and Bredt, 1998) on post- as well as presynaptic sites. On neuronal dendrites, the central core of this matrix is the postsynaptic density (PSD) and it may be assembled in specialized structures, so-called dendritic spines (Figure 1). In the mammalian cortex and hippocampus, most glutamatergic synapses onto excitatory neurons are formed onto such spines (Somogyi et al. 1998, Megías et al. 2001); for this thesis we will concentrate on these prototypic excitatory spine synapses, which represent the majority of excitatory synapses in the mammalian brain.

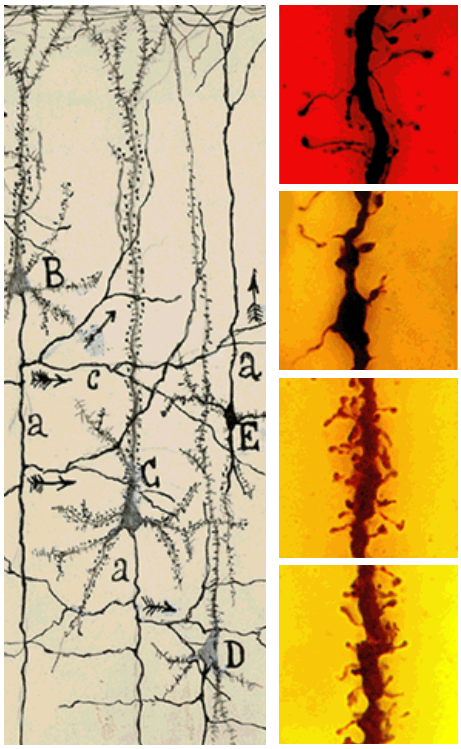

Figure 1. Dendritic spines on human cortical pyramidal cells

Golgi stainings by Cajal. Left: Drawing of pyramidal cells with spinous dendrites (motor cortex). Right: Stainings of pyramidal cell dendrites (frontal cortex). Reassembled from Garcia-Lopez et al. 2010.

Synaptic spines are motile protrusions of the dendritic membrane. They are shaped by actin filaments and often harbour membranous organelles like the endoplasmic reticulum (ER) and endosomes. Mature spines have a bulbous head that is connected to the dendrite via a much thinner spine neck. Due to its architecture and molecular organization, a spine isolates the synapse from the rest of the dendrite and thereby creates a microdomain with respect to protein trafficking, ion diffusion, downstream signalling, and membrane voltage. It is now broadly accepted that spines are plastic and that under physiological conditions their shape and size tends to correlate with synaptic strength and maturity (for review see Sorra and Harris 2000, Nimchinsky et al. 2002, Sheng and Hoogenraad 2007).

1.2 Synapse development and maturation

1.2.1 Synaptogenesis

Synapses are highly adaptive in structure and function. They are actively grown, shrunk, and maintained, and these processes are not only considered a hallmark of early development, but are also believed to be fundamental for learning, memory, and cognition in the mature brain (for review see Hering and Sheng 2001, Calabrese et al. 2006). These processes are controlled by highly complex molecular machineries, and there is evidence that a single synapse harbours a network of more than 1,000 different proteins mutually interacting in an activity-dependent manner (Shinohara 2011). How the assembly of this gigantic multiprotein complex is regulated, has mostly been studied in cell culture systems (for review see McAllister 2007).

The early steps of synapse development are not in the focus of this thesis and only briefly summarized here; the interested reader will find detailled reviews in the literature (Waites et al. 2005, McAllister 2007). Moreover, the timecourse, the order and the precise nature of the molecular events that are involved in early synapse formation are still under debate. This might be due to multiple signalling pathways acting combinatorially, especially in the induction of synaptogenesis (not discussed here, for review see Waites et al 2005). In the early phase of synapse development, pre-and postsynaptic protein precursors will be recruited to sites of axodendritic contacts, which helps to prime and stabilize these sites for synaptogenesis. The presynaptic site of transmitter release, the active zone, is mainly built from pre-assembled complexes travelling in PTVs (**P**iccolo-Bassoon **t**ransport **v**esicles) (Ahmari et al. 2000, Zhai et al. 2001) and STVs (**s**ynaptic vesicle protein **t**ransport **v**esicles, a heterogeneous vesicle population with similarities to synaptic transmitter vesicles) (Sabo et al. 2006). The formation of the postsynaptic specialization seems to be characterized by a more gradual assembly of its components, possibly mirroring the heterogeneity of postsynaptic composition among individual synapses (Bresler et al. 2004, Waites et al. 2005). To which extent these postsynaptic components travel in discrete transport vesicles, as opposed to be recruited from diffuse cytoplasmic protein pools, is not resolved yet (McAllister 2007). Concerning the sequence of molecular assembly, postsynaptic differentiation might be pioneered by Neuroligin-1 (Gerrow et al. 2006), a transsynaptic adhesion molecule. Further early components of the PSD are N-methyl-D-aspartate (NMDA)-type glutamate receptors (Rao et al. 1998, Barrow et al. 2009, Swulius 2010), and scaffold proteins like PSD-95, SAPAP/GKAP (Rao et al. 1998, Gerrow et al. 2006), and Shanks (also known as ProSAPs/Shanks) (Boeckers et al. 1999a, Petralia et al. 2005, Grabrucker et al. 2011).

1.2.2 Synapse maturation

The initial number of synapses formed in the brain is far greater than the number retained, suggesting that synapse elimination (pruning), is a crucial step in normal brain development (Lichtman and Colman 2000). Indeed we know that synapse formation is reversible at all stages and that synapse stability is regulated in an activity-dependent manner (Hua and Smith 2004). This use-dependent activation of immature synapses is a tightly controlled process that becomes manifest both morphologically and functionally (Murakoshi and Yasuda 2012).

Maturing synapses (at least the prototypic excitotory spine synapses this thesis is focused on) expand in size, a process that requires a transsynaptic coordination of pre- and postsynaptic elements (Kay et al. 2011). This growth is correlated to synaptic strengthening, as (1) the number of glutamate receptors is proportional to PSD area and spine volume (Takumi et al. 1999), and (2) PSD area and spine volume are proportional to the area of the active zone and the number of docked vesicles (Schikorski and Stevens 1997). Not only the size, but also the morphology of the dendritic spine is dramatically changing upon maturation (Yuste and Bonhoeffer 2004). In early stages of neural development, most dendritic protrusions are filopodia-like thin, long, motile structures with a half-life of several minutes only (Grutzendler et al. 2002). It is unclear whether these filopodia are direct spine precursors (see Yuste and Bonhoeffer 2004 for discussion), but the developmental disappearance of filopodia coincides with the appearance of persistent spines. These mature spines are typically shorter (less than 2 µm in length), come in mushroom, thin, or stubby shape (Harris et al. 1992), and are increasingly stable with animal age (Grutzendler et al. 2002), possibly encoding life-long memories (Yang et al. 2009).

On the functional level, synapse maturation is characterized by a decrease in transmitter release probablity (Bolshakov and Siegelbaum 1995) and changes in the postsynaptic glutamate receptor composition (Petralia et al. 1999, 2005). The next chapter will describe the latter in more detail, after giving an introduction into the different classes of glutamate receptors.

1.3 Synaptic transmission through glutamate receptors

Glutamate receptors can be classified into two subfamilies according to their structure and signalling properties (for review see Hollmann and Heinemann 1994). Metabotropic glutamate receptors (mGluR1-6) are seven-transmembrane, G-Protein coupled receptors that can activate a range of biochemical signalling cascades and thereby influence neuronal structure and function. Ionotropic glutamate receptors, on the other hand, are permeable to cations and mediate fast synaptic transmission. They can be further subdivided into AMPA, NMDA, and kainate receptors,

according to their respective agonists α-amino-3-hydroxy-5-methyl-4-isoxazolepropionic acid, N-methyl-D-aspartate, and kainic acid. In the well-characterized CA1 pyramidal cells of the mammalian hippocampus (the synapse of interest throughout this thesis), excitatory synaptic transmission relies on AMPA and NMDA receptors (Hollmann and Heinemann 1994, Robinson and Deadwyler 1981). Although these two classes of receptors share fundamental structural similarities, they have distinct functional properties (Table 1), which will be outlined in the following section.

Table 1. Biophysical properties of AMPA and NMDA receptors

Receptor properties depend on subunit composition, thus parameter ranges are given below. Values are taken from Zito and Scheuss (2009) and Dingledine et al. (1999). EC_{50} values were determined for the peak response to rapid application of glutamate.

	AMPAR	NMDAR
rise time	0.2 - 0.4 ms	10 - 50 ms
deactivation	1 ms	50 - 500 ms
glutamate EC_{50}	500 µM	1 µM
single channel conductance	4 - 15 pS	30 - 50 pS

1.3.1 Fast synaptic transmission at excitatory synapses

When glutamate is released from a presynaptic terminal, AMPARs provide rapid depolarization of the postsynaptic membrane, as their kinetics are much faster than the kinetics of NMDARs. Particularly the deactivation kinetics of NMDARs can be very slow, which has a strong impact on the duration of the synaptic current (Lester et al. 1990). Both AMPA and NMDA receptors are selective for cations, but while most AMPARs are not permissive for Ca^{2+} ions (see below), NMDARs have a high Ca^{2+} conductance (MacDermott et al. 1986). This property allows NMDARs to couple synaptic activity to Ca^{2+}-dependent enzymes and downstream signalling pathways that may lead to long-term changes in synaptic strength and structure. NMDAR signalling is regulated, however, by co-agonists (Papouin et al. 2012) and the fact that NMDARs are blocked by Mg^{2+} ions in a voltage-dependent manner (Figure 2). Only if the postsynaptic membrane is sufficiently depolarized, the Mg^{2+} block will be relieved from the channel pore and ion flux will be allowed upon binding of glutamate (Nowak et al. 1984).

During early postnatal development, many neurons form synapses that harbour NMDA but not AMPA receptors (Liao et al. 1995, Isaac et al. 1995, Durand et al. 1996, Nusser et al. 1998, Wu et al. 1996, Isaac et al. 1997, Rumpel et al. 1998, Franks and Isaacson 2005). These synapses are postsynaptically silent, as they only allow synaptic transmission to occur if the postsynaptic membrane is depolarized and the Mg^{2+} block is released from the NMDAR channel pore. It has

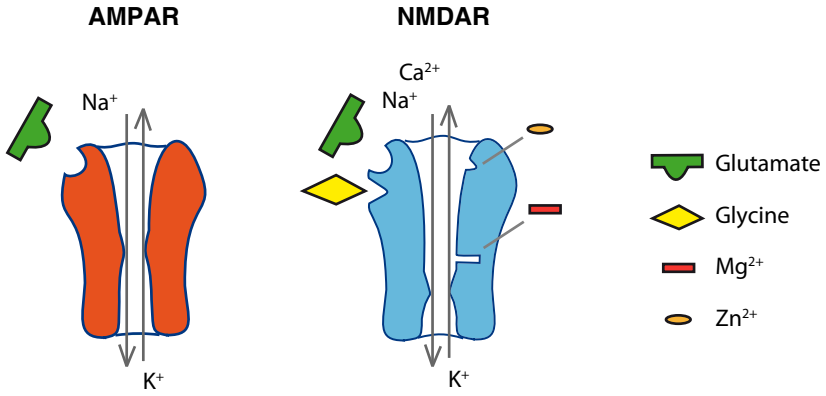

Figure 2. Properties of glutamate receptors

AMPARs and NMDARs both permit the flow of Na^+ and K^+ ions upon glutamate binding. In addition, NMDARs can pass Ca^{2+} ions, are blocked by Mg^{2+} and Zn^{2+} in a voltage-dependent manner, and require a co-agonist (glycine or D-serine).

been shown that coincident pre- and postsynaptic activation can unsilence these synapses by NMDAR-triggered insertion of AMPARs into the postsynaptic membrane (Isaac et al. 1995, Liao et al. 1995, Durand et al. 1996).

1.3.2 Molecular characteristics of NMDA receptors

NMDARs are heterotetramers. Their agonist affinity, Ca^{2+} permeability, ion conductance, channel kinetics, and sensitivity to Mg^{2+} block are dependent on NMDAR subunit composition and posttranslational modifications. NMDARs are assembled from at least one obligatory GluN1 subunit and a complement of GluN2 subunits (GluN2A–D) (Monyer et al. 1992, Ishii et al. 1993). The GluN2 subunits determine the current kinetics (Monyer et al. 1994, Vicini et al. 1998), and are thought to initiate differential intracellular signalling (Barria and Malinow 2005, Kim et al. 2005, Foster et al. 2010). The expression of GluN2 subunits is developmentally regulated. During embryonic and early postnatal development, principal neurons in the hippocampus and neocortex mostly contain NMDARs assembled from two GluN1 and two GluN2B subunits (Watanabe et al. 1992, Monyer et al. 1994, Sheng et al. 1994). In the course of synaptic maturation, the GluN2B-containing NMDARs are partially substituted by those containing the GluN2A subunit (Monyer et al. 1994, Sheng et al. 1994, Petralia et al. 2005); heterotrimeric receptors most likely occur as well (Rauner and Köhr 2011, Gray et al. 2011). This subunit switch fastens NMDAR kinetics (Hestrin 1992, Carmigniotto et al. 1992, Monyer et al. 1994, Flint et al. 1997) and thus has implications for synaptic integration (Singh et al. 2011). Besides that, the differential coupling of GluN2A and GluN2B subunits to intracellular signalling pathways is thought to raise the induction threshold for LTP (Barth and Malenka 2001, Gray et al. 2011). There is also evidence that NMDARs can be activated at extrasynaptic sites, where they might induce signalling that negatively regulates synaptic strength and cell survival (Groc et al. 2009, Newpher and Ehlers 2009, Hardingham and Bading 2010).

1.3.3 Molecular characteristics of AMPA receptors

Neurons are equipped with a rich repertoire of AMPARs, a result of differential subunit assembly and a variety of posttranslational modifications (namely alternative splicing and RNA editing) (Hollmann & Heinemann 1994). In addition, the molecular complexity of AMPARs is amplified by their co-assembly with various transmembrane auxiliary subunits, which modulate receptor trafficking and gating (reviewed in Tomita 2010). The best characterized AMPAR auxiliary subunit is stargazin, a TARP (**t**ransmembrane **A**MPAR **r**egulatory **p**rotein) family protein, which modulates receptor gating and is crucial for the trafficking as well as anchoring of AMPARs to the PSD.

The protein products of the four AMPAR subunits GluA1–4 share homology and domain organization (reviewed in Nakagawa 2010); they form tetramers that assemble as dimers of dimers with various subunit stochiometries (Mano and Teichberg 1998, Rosenmund et al. 1998, Mansour et al 2001). Channel gating kinetics are tuned over a fivefold range, depending on the subunit type and RNA processing events within the ligand-binding domain (Greger and Esteban 2007): Alternative splicing results in flip/flop isoforms of GluA1-GluA4 (Sommer et al. 1990), GluA2-GluA4 mRNAs are edited at the R/G site (Lomeli et al. 1994). Both alterations accelerate desensitization and resensitization in a developmentally regulated manner, with faster channels emerging later in ontogeny (Greger and Esteban 2007).

RNA-processing also modulates channel assembly and trafficking properties. GluA2 subunits are additionally edited at their ion selectivity filter in the transmembrane domain, the Q/R site (Sommer et al. 1991). The vast majority of endogenous GluA2 subunits are edited to the R form (Puchalski et al. 1994), which has important implications for AMPAR assembly and physiology: Edited GluA2 subunits favour to assemble with unedited AMPAR subunits (Greger et al. 2003), and subsequently dominate the properties of the resulting heterotetramer (Figure 3). The presence of GluA2 subunits renders AMPARs Ca^{2+}-impermeable (Hollmann et al. 1991) and drastically decreases their conductance (Swanson et al. 1997), making GluA2 a critical subunit for the regulation of synaptic AMPAR signalling. In addition, Ca^{2+}-permeable AMPARs that lack the GluA2 subunit are blocked by intracellular polyamines at depolarized potentials (Verdoorn et al. 1991). The fact that this block can be released upon intense synaptic activity further increases the computational power of synaptic transmission.

Immunoprecipitation studies suggest that CA1 pyramidal neurons harbour primarily GluA1/2 and GluA2/3 heteromers, very few GluA1/GluA3 heteromers, and less than 10 % GluA1 homomers (Wenthold et al. 1996). A recent study, however, used a genetic approach and found the vast majority of synaptic and extrasynaptic receptors to be GluA1/GluA2 heteromers

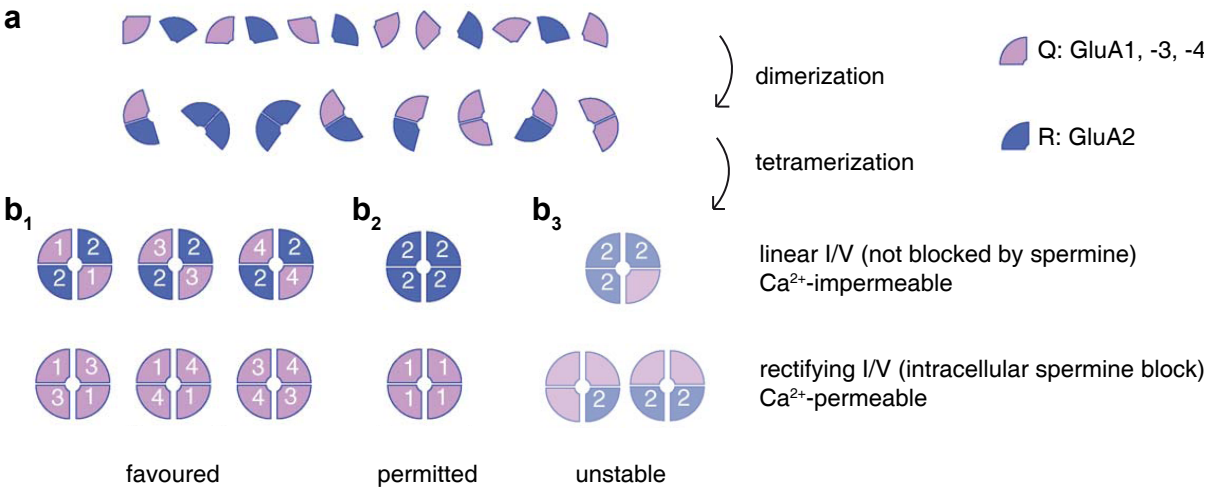

Figure 3. AMPAR subunit stochiometries

Schematic representation of subunit partnerships involved in AMPAR formation. The colour code refers to the editing state at the Q/R site (see legend upper right). **a**. Subunits are synthesized in the ER. Formation of heteromeric dimers is favoured, but homomeric dimers are also allowed. **b**. Tetramerization by dimer of dimer formation. According to the observation that pairs of identical heterodimers preferentially co-assemble (Mansour et al. 2001), subunit combinations with a symmetrical stochiometry will be favoured. b_1. Combinations of differentially edited subunits are favoured, as a result of which many AMPARs contain the GluA2 subunit (Greger et al. 2003) and are Ca^{2+}-impermeable (top). However, GluA2-lacking, Ca^{2+}-permeable combinations are also possible if they are favoured by structural differences between AMPAR subunits like flip vs. flop isoforms (bottom) (Brorson et al. 2004). b_2. Homomeric assemblies differing in flip–flop isoform are also permitted. b_3. Mosaic AMPAR subtypes with a single copy of GluA2, two copies of GluA2 in close juxtaposition, or three GluA2 subunits are unstable. Modified from Cull-Candy et al. 2006.

(Lu et al. 2009). This study also argued against the presence of Ca^{2+}-permeable synaptic GluA1 homomers, the existence of which has been demonstrated soon after using yet another approach (Rozov et al. 2012). In conclusion, it seems justified to say that this issue awaits further investigation. How the different AMPAR subunits might help to shape synaptic dynamics will be outlined in section 1.4.2.

1.4 Postsynaptic protein networks shape the spine

Dendritic spines function as semi-autonomous signalling units that modify their properties in accordance to the presynaptic input they receive. To do so, spines harbour complex protein networks that can be understood as highly interconnected functional modules (Figure 4). These modules and some of their most important functions will be described in the following sections.

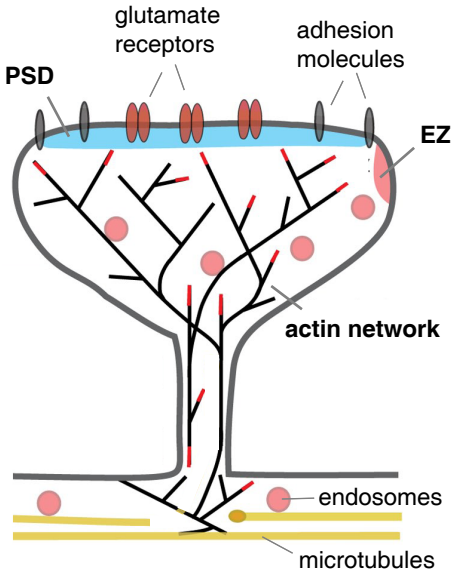

Figure 4. Functional modules of dendritic spines

Schematic diagram of a mushroom spine. The postsynaptic density (PSD, blue) anchors adhesion molecules (gray) and glutamate receptors (brown). The endocytic zone (EZ, pink) is located in extrasynaptic regions; recycling endosomes (pink circles) are found in shaft and spine. Dendritic spines contain a continuous network of actin filaments (black), which undergo extensive branching at the neck–head junction and are highly branched throughout the spine head. Growing ends of actin filaments are indicated in red. Stable microtubule arrays are predominantly present in the dendritic shaft. Membranous organelles like the smooth endoplasmic reticulum, a spine apparatus, or polyribosomes can be found in subsets of spines as well, but are not illustrated here. Modified from Hotulainen and Hoogenrad 2010.

1.4.1 Functional modules of dendritic spines

Among the protein networks within dendritic spines, the postsynaptic density (PSD) attracted much attention as a hallmark of excitatory synapses in electron micrographs (Gray 1959). Occupying only 10 % of the spine surface area, the PSD contains hundreds of protein components (Bayés et al. 2011, Shinohara et al. 2011) and can be envisioned as a collection of supramolecular complexes serving to maintain and modulate synaptic function (reviewed in Kennedy 2000, Murakoshi and Yasuda 2012). The PSD has a central role in the anchoring of synaptic glutamate receptors, the clustering of transsynaptic adhesion molecules, and the coupling of synaptic activity to intracellular signalling cascades and the actin cytoskeleton (Figure 5) (reviewed in Ziff 1997, Craven and Bredt 1998, Kennedy 2000, Sheng and Pak 2000, Boeckers 2006). Among the most prominent components of the PSD are CamKII (a Ca^{2+}-dependent protein kinase), PSD-95 family proteins (molecular anchors for NMDA and AMPA receptors), and Shanks. The latter two are PDZ (PSD-95/DLG/ZO-1) domain-containing scaffold proteins which are thought to organize the PSD both structurally and functionally (reviewed in Kim and Sheng 2004, Feng and Zhang 2009). Moreover, these scaffold proteins couple the PSD to other functional modules within the spine, like the actin cytoskeleton (discussed in section 1.4.3) or the endocytic zone (EZ). EZs are clathrin-coated membrane domains that are present in a subset of spines (Cooney et al. 2002), where they are stabilized adjacent to the PSD via a chain of protein-protein interactions involving Dynamin-3, Homer, and Shanks (Blanpied et al. 2002, Rácz et al. 2004, Lu et al. 2007). The endocytic machinery is thought to be responsible for the localized endocytosis of AMPARs, the functional role of which will be discussed in the following section.

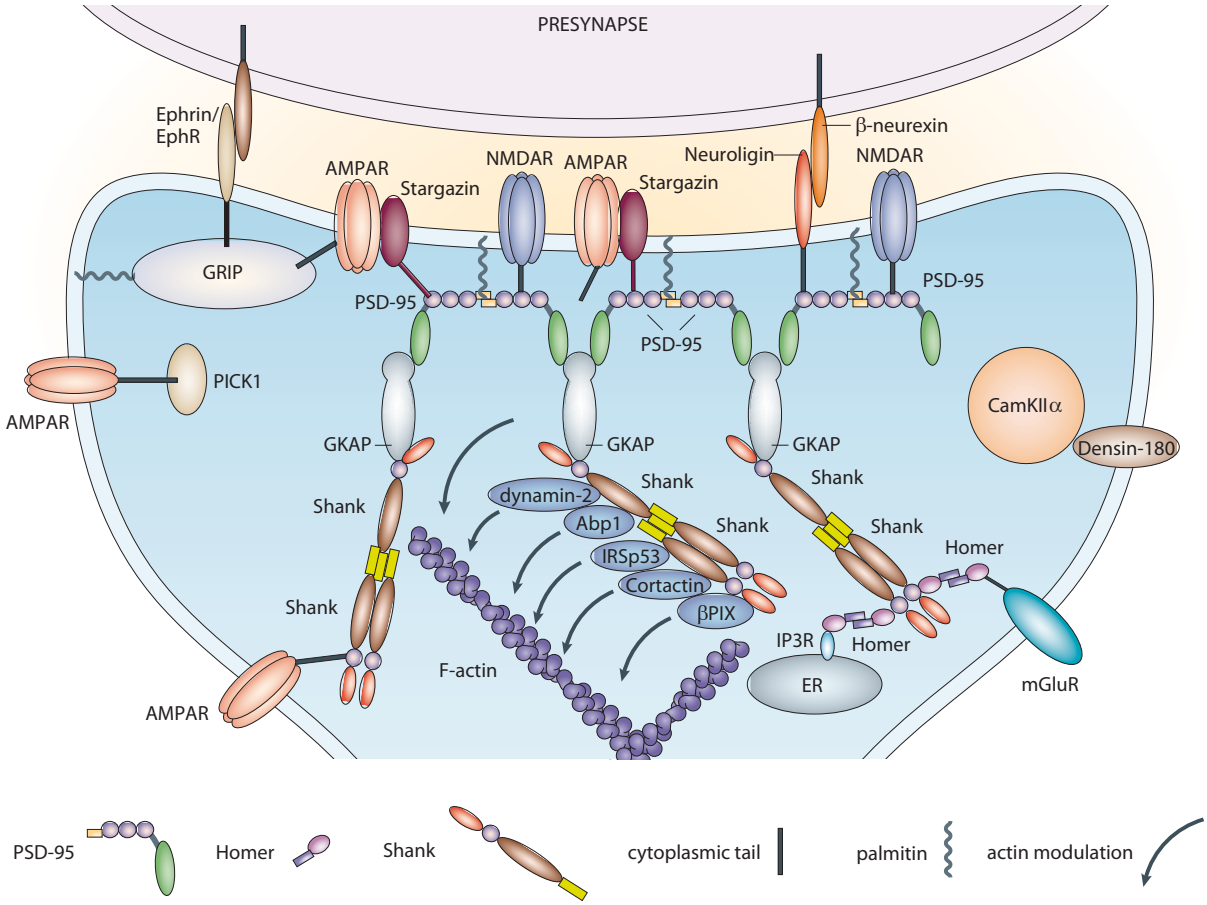

Figure 5. Molecular components of the PSD.

A selection of proteins and protein-protein interactions are depicted to illustrate the organization of the PSD, the synaptic anchoring of glutamte receptors, and the modulation of the actin cytoskeleton. Multimerization and domain structure is indicated for the scaffold proteins PSD-95, Shank and Homer. Modified from Kim and Sheng (2004).

1.4.2 The trafficking of ionotropic glutamate receptors

Many neurons regulate their synaptic AMPAR equipment in an activity-dependent fashion. In the connections from CA3 to CA1 pyramidal cells, this is reflected by a large heterogeneity of synaptic strength among different synapses onto one particular pyramidal cell (Nusser et al. 1998). To allow for dynamic regulation, synaptic AMPARs are highly non-static. They constantly cycle into and out of the neuronal membrane (Lüscher et al. 1999) and diffuse laterally between intra- and extrasynaptic membrane regions (Borgdorff and Choquet 2002). A wealth of chaperones, auxiliary subunits, and scaffolding molecules assists in constantly trafficking AMPARs into and out of synapses (reviewed in Barry and Ziff 2002, Malinow and Malenka 2002, Anggono and Huganir 2012). The precise nature of these trafficking events is critically dependent on AMPAR subunit composition, as the intracellular C-terminal tails of GluA1-4 can couple to distinct trafficking pathways (Figure 6, inset). Specifically, GluA3 and the predominant splice form of GluA2 share homology in their cytoplasmic tails, of which the last

four amino acids constitute a group II PDZ ligand. While that confers binding to PICK1 and GRIP, the GluA1 subunit binds to SAP97 and Shank proteins via its C-terminal group I PDZ ligand. In addition, 4.1 proteins have been identified as adaptors for GluA1, and NSF is known to bind the GluA2 subunit (reviewed in Malinow and Malenka 2002, Anggono and Huganir 2012).

The functional implications of these interactions have been investigated in a series of studies (Shi et al. 1999, Hayashi et al. 2000, Heynen et al. 2000, Passafaro et al. 2001, Shi et al. 2001), giving rise to the generally accepted model for AMPAR trafficking in CA1 pyramidal cells that is depicted in Figure 6: GluA2/3 heteromers have a role in basal synaptic transmission, they are highly mobile and undergo continuous exo-/endocytotic cycling that depends on their interaction with NSF. Strong synaptic activity recruits additional GluA1/2 receptors to synapses via an alternative trafficking pathway (Hayashi et al. 2000, Passafaro et al. 2001). This might result in an expansion of the PSD and/or increase the number of AMPAR slots that are available in the postsynaptic scaffold. These slots might subsequently be filled by GluA2/3 receptors, which continue to cycle into and out of the synaptic membrane (Shi et al. 2001). The model derives further credit from the observations that LTP is absent in mice lacking the GluA1 subunit (Zamanillo et al. 1999) but not in mice lacking GluA2 (Jia et al. 1996), consistent with the idea that *de novo* insertion of synaptic AMPARs depends on GluA1, but not GluA2.

AMPAR cycling mechanisms are also exploited for the downscaling of synaptic strength, a phenomenon called LTD (long-term depression). LTD can be triggered by various stimuli like AMPAR, NMDAR and mGluR activation that seem to converge mechanistically (Scholz et al. 2010). Subsequent changes in the phosphorylation state of AMPAR subunits (affecting both GluA1 and GluA2) have been described to be instrumental for the induction of LTD (Malenka and Bear 2004, Gladding 2009). These changes may reduce the receptor‘s open probability (Banke et al. 2000) and/or alter the binding of AMPARs to their scaffold proteins. Eventually, AMPARs are removed from the postsynaptic membrane via endocytosis (Malinow and Malenka 2002, Malenka and Bear 2004) which is, in contrast to constitutive AMPAR cycling, dependent on the clathrin adaptor AP2 and independent of NSF (Lee et al. 2002). Expression of LTD can thus reduce the steady-state number of AMPARs, the maintenance of which might again be dependent on slot proteins (Malenka and Bear 2004).

Different AMPAR subtypes like GluA1/2 and GluA2/3 heteromers not only have different protein adaptors and insertion triggers (Shi et al. 2001, Passafaro et al. 2001), but are also trafficked from different endosomal pools under control of specific molecular effectors (Brown et al. 2007). The mechanistic repertoire for the modulation of synaptic strength is further extended by intracellular signalling cascades that determine the fate of internalized AMPARs. AMPARs in

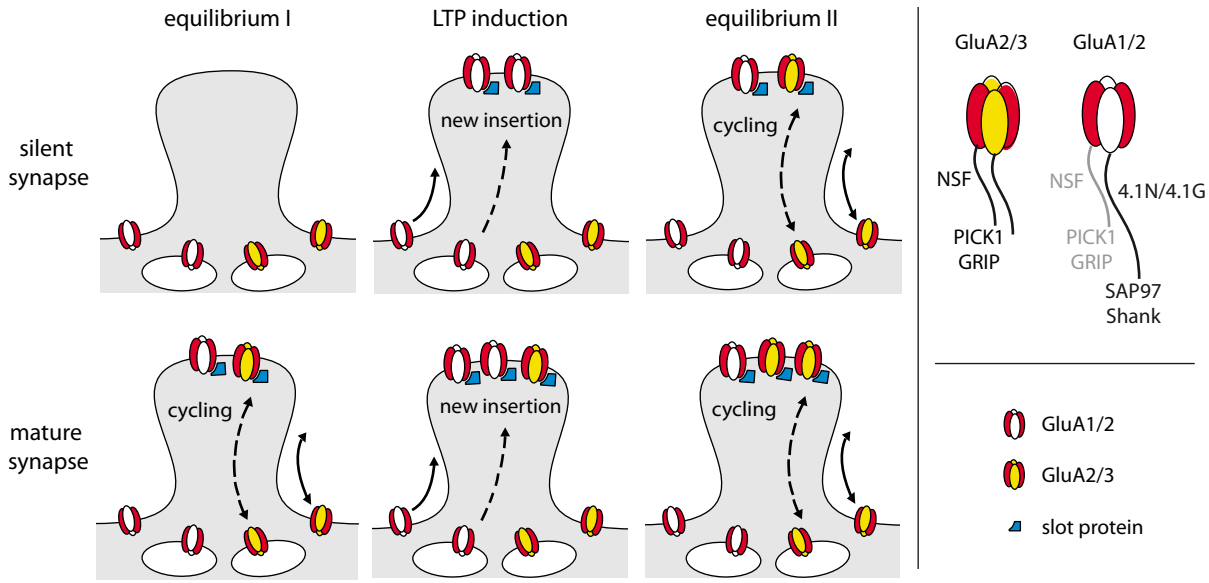

Figure 6. AMPAR subunits are differentially trafficked at rest and during LTP

Under baseline conditions („equilibrium I"), constitutive AMPAR cycling maintains a dynamic equilibrium of synaptic glutamate receptors. Upon activation of NMDARs („LTP induction", NMDARs not shown), GluA1/2 heteromers are delivered into the synapse, where they are subsequently replaced by GluA2/3 heteromers. A new stable state („equilibrium II") is reached, again maintained by a balanced cycling of receptors into and out of synapses. The synaptic insertion of AMPARs occurs through lateral diffusion (arrows) and possibly also via direct synaptic exo- and endocytosis (dotted arrows). The box in the upper right corner illustrates the molecular adaptors available for GluA2/3 heteromer trafficking and how this repertoire changes in the presence of the dominant GluA1 subunit (Shi et al. 2001, Passafaro et al. 2001). Modified and extended from Barry and Ziff 2002.

recycling endosomes can be re-inserted into the membrane or targeted to lysosomes, depending on the conditions of AMPAR endocytosis (Ehlers 2000, Lin et al. 2000, Fernandez-Monreal et al. 2012).

The localization of AMPARs to synapses is believed to happen primarily via dendritic insertion with subsequent lateral diffusion and synaptic trapping (Borgdorff and Choquet 2002, Adesnik et al. 2005, Yudowski et al. 2007, Yang et al. 2008, Lin et al. 2009, Makino and Malinow 2009). However, there is evidence to suggest a role for the spine endocytic machinery in this process (Jaskolski et al. 2009), and some researchers follow the hypothesis that a significant portion of AMPARs might be introduced into the synaptic membrane by direct exocytosis of receptor-containing vesicles (Kennedy et al. 2010, Patterson et al. 2010). In an attempt to consolidate these diverging views, Czöndör and colleagues (2012) recently developed a biophysical model in which they suggest the coexistence of both insertion modes. In this framework, AMPARs are trafficked into synapses mainly via diffusion from extrasynaptic sites, while the direct exocytosis of AMPARs is a potent mechanism available to a certain fraction of synapses only.

1.4.3 Dynamics of the actin cytoskeleton

Actin filaments (F-actin) are dynamically assembled from monomeric G-actin and subject of constant turnover. In synaptic spines, the majority of actin filaments is extensively branched and highly dynamic, with turnover times of less than a minute (Star et al. 2002), allowing spines to be highly mobile structures (Fischer et al. 1998, Lendvai et al. 2000). Actin-binding proteins are modulating F-actin dynamics, filament branching, and the cross-linking of F-actin to other cytoskeletal networks. These modulatory proteins are coordinated by calcium regulatory mechanisms and cellular signalling machineries (reviewed in Hotulainen and Hoogenraad 2010). The actin-signalling pathways in spines are regulated by synaptic receptors such as NMDA and AMPA receptors (Fischer et al. 2000), but also other receptors and adhesion molecules. The major signalling hubs in actin cytoskeleton regulation are small GTPases of the Rho and Ras family which coordinate the function of actin-binding proteins (reviewed in Hotulainen and Hoogenraad 2010).

Long-term changes in synaptic efficacy are often accompanied by actin-driven structural plasticity (reviewed in Cingolani and Goda 2008, Murakoshi and Yasuda 2012). However, neurons not only exploit actin dynamics to control spine shape, but also to coordinate other processes: Actin dynamics are involved in the organization of the PSD, the anchoring of AMPARs, and the facilitation of AMPAR exo-/endocytic cycling (reviewed in Cingolani and Goda 2008, Frost et al. 2010). When actin polymerization is blocked, PSDs lose a substantial fraction of AMPARs and scaffold proteins (Allison et al. 1998, Kuriu et al. 2006), suggesting that the PSD is not a cohesive structure tied together by the intermolecular binding of scaffold molecules. Instead, the PSD might be organized as an assembly of partially autonomous functional subsets (Frost et al. 2010).

Morphological and functional synaptic plasticity often are, but must not necessarily be linked to one another. Neither everywhere in the brain nor under all circumstances are changes in synaptic strength associated with changes in spine size (Sdrulla and Linden 2007, Wang et al. 2007). Thus, whenever neurons like CA1 pyramidal cells scale their spine size to synaptic strength (Nusser et al. 1998, Matsuzaki et al. 2004, Noguchi et al. 2005), they must have mechanisms in place to coordinate both forms of plasticity. Similar to the induction of long-term plasticity, structural rearrangements of actin filaments in dendritic spines are dependent on NMDAR activation (Fukazawa et al. 2003, Zhou et al. 2004). Furthermore, actin polymerization in dendritic spines is known to be required but not sufficient for NMDAR-dependent LTP (Kim and Lisman 1999, Krucker et al. 2000, Fukazawa et al. 2003, Wang et al. 2007). The signalling pathways leading to structural and functional synaptic plasticity, however, can diverge considerably and may even be dissociable (Zhou et al. 2004, Wang et al. 2007). An elegant model to

explain the coordination of morphological and functional plasticity is centered around AMPARs: Spine morphology apparently scales to the expression level of GluA2 (Passafaro et al. 2003), a mechanism that depends on the GluA2 subunit's extracellular domain and possibly involves interactions with N-Cadherin (Saglietti et al. 2007). Along the same lines, Kopec and colleagues (2007) showed that spine enlargement upon LTP induction depends on (1) the translocation of the GluA1 cytoplasmic tail into the PSD, and (2) on the presence of an intact PDZ-domain at the tails c-terminus. According to this finding, GluA1 incorporation into synapses would not only provide for an increase in synapse strength, but also serve as a molecular adaptor to induce modifications of the spine cytoskeleton; this coordination might be stabilized by extracellular receptor-ligand interactions of GluA2.

1.5 Shank proteins interconnect postsynaptic modules

The previous chapter has illustrated how complex protein interaction networks allow for the structural and functional integrity and plasticity of synapses. In this chapter, we will introduce the Shank family of scaffold proteins and present some ideas as to how these proteins might help to organize synaptic protein networks.

1.5.1 Shank proteins: A family picture

Shank proteins are prominent constituents of the PSD in excitatory synaptic spines (reviewed in Sheng and Kim 2000, Boeckers et al. 2002, Kreienkamp 2008). The Shank family comprises three genes, the products of which we refer to as Shank1, Shank2, and Shank3, although alternative names exist and are in use (Table 2).

Table 2. Terminology of the Shank protein family

The three Shank genes were independently cloned and named by several research groups. Grey fonts refer to terminology not in use anymore. Terminology used in this thesis is written in bold.

Naisbitt et al. 1999 **SH**3- and **ank**yrin-containing proteins	**Shank1**	**Shank2**	**Shank3**
Boeckers et al. 1999a, 1999b **pro**line-rich **s**ynapse-**a**ssociated **p**rotein		ProSAP1	ProSAP2
Tobaben et al. 2000	Spank-1	Spank-3	Spank-2
Du et al. 1998 **c**ortactin **b**inding **p**rotein		CortBP1	
Yao et al. 1999	Synamon		
Zitzer et al. 1999 **s**omato**st**atin **r**eceptor **i**nteracting **p**rotein	SSTRIP		

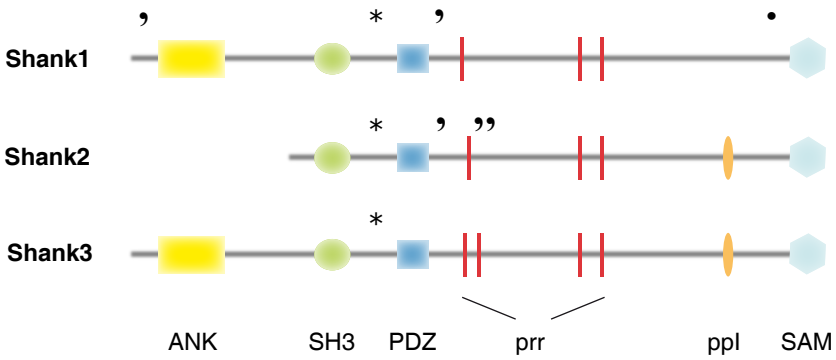

Figure 7. Shank protein domain structure

Sites of alternative splicing are indicated by commata (exon insertion sites), asterisks (alternative transcription start), full stops (alternative stop codon). ANK: ankyrin repeats. ppI: polyproline I helix.

Shank proteins are large (~ 2000 amino acids, 200 kDa) and contain multiple protein–protein interaction domains which are highly conserved among all Shank family members (Figure 7). Although domain composition can be differentially regulated via alternative splicing events, most Shank isoforms found at the PSD of excitatory synapses contain an SH3 (Src homology 3) domain, a PDZ domain, a SAM (sterile alpha motif) domain and a proline-rich region (prr). Moreover, all family members can harbor Ankyrin repeats, although the respective Shank2 splice variant has been detected in liver tissue only (McWilliams et al. 2004).

All Shank proteins can be found in the brain, but only Shank1 seems to be brain-specific (Lim et al. 1999). Shank2 is expressed in neurons, some glia, endocrine cells and can be detected in liver and kidney (Redecker et al. 2001). Shank3 mRNA was identified at different levels in all tissues (Lim et al. 1999). In the brain, all three Shanks are coexpressed in the cortex and the hippocampus; other brain regions show differential expression of individual isoforms (Boeckers et al. 2004). The localization of mRNAs is cell-type specific as well: In the hippocampus, a dendritic localization of mRNAs was observed for Shank1 and Shank3 only, whereas Shank2 (and Shank1) transcripts can be found in the dendrites of cerebellar purkinje cells (Zitzer et al. 1999, Boeckers et al. 2004). All three family members are present at the PSD of excitatory synapses (Boeckers et al. 1999a, Boeckers et al. 1999b, Naisbitt et al. 1999), where they reside in deeper layers than PSD-95 and SAPAP/GKAP (Valtschanoff and Weinberg 2001). During development, Shanks initially accumulate in the cytoplasm of somata and growth cones; localization to the PSD is observed between postnatal day (P)6 and P10 with different time courses and trafficking mechanisms for the different Shanks: Shank1 needs the PDZ domain for synaptic targeting (Sala et al. 2001) and it localizes to the PSD after formation of the PSD-95/GKAP complex (Naisbitt et al. 1999, Sheng and Kim 2000). In contrast, Shank2 and Shank3 localization to synapses depends on the SAM domain (Boeckers et al. 2005) and occurs very early during synaptogenesis, with Shank2 preceding the incorporation of the PSD-95/NMDA complex (Boeckers et al. 1999a) and Shank3 being transported with it (Gerrow

et al. 2006). These findings have recently been confirmed and extended by the observation that the scaffolding function of Shank2 and Shank3, but not Shank1, is modulated by zinc ions (Grabrucker et al. 2011).

1.5.2 The interaction network of Shank family proteins

By virtue of their multiple protein–protein interaction domains (Figure 7), Shanks can interact with proteins that are involved in a wide range of synaptic processes. Many interactions have been described so far (a selection of them is presented in Table 3), more are likely to follow. In general, Shanks are thought to be positive regulators of spine development and maturation (Sala et al. 2001, Roussignol et al. 2005). More precisely, Shanks have a role in the coordination of actin dynamics (Du et al. 1998, Soltau et al. 2002, Qualmann et al. 2004, Kim et al. 2009, Durand et al. 2011), they couple to scaffolds of ionotropic (Boeckers et al. 1999b, Nasibitt et al. 1999) as well as metabotropic glutamate receptors (Tu et al. 1999, Verpelli et al. 2011), they connect to the endocytic machinery (Okamoto et al. 2001, Lu et al. 2007) and Ca^{2+} signalling (Sala et al. 2005, Hwang et al. 2005). They can also modulate CREB signalling by clustering of Ca^{2+} channels (Zhang et al. 2005) and recruitment of metabotropic glutamate receptors (Verpelli et al. 2011).

1.5.3 Aim of this study

As outlined in the previous section, Shanks are PSD scaffolds with the ability to interconnect a broad spectrum of signalling pathways in synaptic spines. These interactions are also interesting from a pathophysiological point of view, as mutations in *SHANK* genes have been found in patients with autism and/or mental retardation (Durand et al. 2007, Berkel et al. 2010, Sato et al. 2012), and alterations of Shank scaffolds have been observed in patients with Alzheimer‘s disease (Gong et al. 2009, Roselli et al. 2009, Pham et al. 2010).

Fuelled by the implication of Shanks in neurodevelopmental disorders, several research groups made the effort to generate knockout mouse lines for the three *Shank* genes. Such forward genetic approaches were hoped to help elucidate which protein functions and interactions would actually impact neuronal physiology. Before and during the work on this thesis, several such studies were published on Shank1 and Shank3 (Hung et al. 2008, Peca et al. 2011, Wang et al. 2011, Yang et al. 2012). The main findings on the molecular, structural, and physiological level are condensed in Table 4.

Table 3. Interaction partners of Shank proteins

For each Shank protein domain, the binding partners with their respective binding motifs and the functional implications are listed. The superscript abbreviations [S1] (Shank1), [S2] (Shank1), and [S3] (Shank3) indicate the family member the interaction has been demonstrated for. The abbreviation is put in brackets, if an interaction is probable (full conservation of the binding sequence), but has not been tested. An asterisk (*) indicates that the other isoforms have not been tested for interaction. Further information on underlined key words can be found in the glossary.

DOMAIN	INTERACTS WITH	MOTIF	FUNCTIONAL IMPLICATION	REFERENCES
ANK	α-fodrin (αII-spectrin) [S1,S3]	C-terminal spectrin repeat 21	α-fodrin binds to actin and calmodulin	Boeckers et al. 2001
	sharpin [S1,*]	aa 172-305	sharpin binds to α1-integrin, β1-integrin	Lim et al. 2001
PDZ (type I)			The PDZ domain is essential for the synaptic localization of Shank1.	Sala et al. 2001
	GKAP/SAPAP [S1,S2,S3]	C-terminus (QTRL)	coupling to AMPARs, NMDARs, and cell adhesion molecules via PSD-95	Naisbitt et al. 1999, Boeckers et al. 1999b, Yao et al. 1999
	GluA1 [S1,S2,S3]	C-terminus (ATGL)	GluA1 trafficking is disturbed in Shank3$^{-/-}$ mice	Uchino et al. 2006
	βPix [S1,S2,S3]	C-terminal leucine zipper	βPix is a guanine nucleotide exchange factor (GEF) for Rho GTPases and thus modulates actin dynamics	Park et al. 2003 Saneyoshi et al. 2008, 2010
	ProSAPiP1 [S3,*]	C-terminus	ProSAPiP1 binds to SPAR, a GTPase activating protein (GAP) that modulates actin dynamics via RhoGTPases	Wendholt et al. 2006
	Phospholipase C β3 [S2,*]	C-terminus	modulation of mGluR-mediated Ca^{2+} signalling	Hwang 2005
	CIRL [S1,S2,*] SSTR2 [S1,*]	C-terminus	CIRL and SSTR2 (somatosstatin receptor 2) are G-Protein-coupled receptors (GPCRs) that activate intracellular signalling cascades	Zitzer et al. 1999, Kreienkamp et al. 2000, Tobaben et al. 2000
	Shank proteins	PDZ (free and complexed)	antiparallel dimerization	Im et al. 2003

Table 3. Interaction partners of Shank proteins (continued)

DOMAIN	INTERACTS WITH	MOTIF	FUNCTIONAL IMPLICATION	REFERENCES
PDZ + SH3	$Ca_V1.3a$ S1,S3 *	C-terminus (ITTL), C-terminal -PXXP-	Ca^{2+} influx via $Ca_V1.3a$ can induce CREB signalling	Zhang et al. 2005
prr	dynamin-2 S1,S2,*	C-terminal PRR	Dynamin-2 is a small GTPase with a role in membrane fission. In concert with cortactin, dynamin-2 modulates actin dynamics	Okamoto et al. 2001 Schafer et al. 2002
	Abp1 S2, S3, motif not conserved in S1	SH3 domain	Abp1 binds to F-actin and modultes its dynamics	Qualmann et al. 2004
	IRSp53 S1, S3 *	SH3 domain	IRSp53 is bound by the activated Rho GTPase cdc42 and connects to PSD-95	Bockmann et al. 2002, Soltau et al. 2002
	SPIN90 S1, S2, S3	proline-rich domain	SPIN90 modulates actin dynamics and binds to PSD-95	Kim et al. 2009
prr -PPLEF- S2,S3 -PPEEF- S1	Homer (all isoforms) S1, S2, S3	EVH1 domain	Homer crosslinks group I mGluRs, modulates IP_3-receptor dependent Ca^{+2} release from the ER, and binds to dynamin-3, which has a role in postsynaptic AMPAR endocytosis.	Tu et al. 1999 Hwang et al. 2005 Hayashi et al. 2009
ppl -KPPVPPKPK-	Cortactin S2, S3	SH3 domain	Cortactin has a role in stabilization and branching of actin filaments via interactions with F-actin and Arp2/3.	Du et al. 1998, Naisbitt et al. 1999 Trachentberg et al. 2002
SAM	The SAM domain is essential for the synaptic localization of Shank2 and Shank3			Boeckers et al. 2005
	Shank proteins	SAM	oligomerization	Naisbitt et al. 1999

Table 4. Deletion studies involving *Shank* genes

Published knockout mouse lines for *Shank1* and *Shank3*. The first coloumn contains information on the brain region investigated, the age of animals tested as well as the publication reference. The following coloumns contain information on the molecular, structural, and physiological phenotype of the respective mouse model.

MODEL	MOLECULAR	STRUCTURAL	PHYSIOLOGICAL
Shank1$^{-/-}$ hippocampus 3-4 weeks Hung et al. 2008	reduced level of GKAP, Homer	smaller and fewer spines thinner PSDs	reduced synaptic transmission (fEPSP input/output, mEPSC frequency) normal synaptic plasticity (LTP: 1x HFS) normal A/N ratio
Shank3B$^{-/-}$ striatum* 5-9 weeks Peça et al. 2011	reduced level of Homer, PSD-93, GluA2, NR2A, NR2B	smaller and fewer spines increased dendritic complexity	reduced synaptic transmission (fEPSP input/output, mEPSC frequency and amplitude) normal A/N ratio
	*: physiology in hippocampal CA1 showed no differences in fEPSPs, mEPSCs		
Shank3$^{e4\text{-}9\ -/-}$ hippocampus 2-4 month Wang et al. 2011	reduced level of Homer1b/c, GKAP, GluA1	longer and fewer spines[2]	normal synaptic transmission reduced LTP (2x HFS) reduced GluA1 insertion in chemical LTP
	*: Spines were different in adolescent but not adult mice (4 weeks vs 10 weeks)		
Shank3$^{ank\ -/-}$ hippocampus 4-6 weeks Yang et al. 2012*			reduced synaptic transmission (fEPSP input/output) reduced LTP (TBS), normal LTD
	*: The mouse line was initially published by Bozdagi et al. (2010), the electrophysiological phenotype in the -/- mice is reported by Yang et al. (2012).		

Two of these studies (Peça et al. 2011, Yang et al. 2012) were primarily designed to explore the role of Shanks in neurodevelopmental disorders and thus focused on the behavioural phenotypes of the transgenic mice. The other two studies more extensively investigated and discussed the physiological role of Shanks: Hung and colleagues (2008) hypothesized a role for Shank1 in the stabilization of mature spines, as they found a reduction of basal synaptic transmission without impairment in LTP. Wang et al. (2011) proposed a role for Shank3 in the trafficking of GluA1-containing AMPARs, resulting in reduced LTP in Shank3$^{e4\text{-}9\text{-}/\text{-}}$ mice.

The aim of this thesis was the electrophysiological analysis of Shank2$^{-/-}$ mice, a mouse line generated in the laboratory of Tobias Böckers (Ulm University, Germany). We wanted to know whether basal synaptic transmission and plasticity was altered in these mice and performed

an electrophysiological investigation of their synaptic properties in the CA1 region of the hippocampus. Considering the role of Shank proteins in neurodevelopmental disorders, we did so with a focus on different developmental stages.

2 Materials and Methods

2.1 Materials

Chemical solutions

Slicing ACSF contained (in mM): 87 NaCl, 26 $NaHCO_3$, 50 sucrose, 25 glucose, 3 $MgCl_2$, 2.5 KCl, 1.25 NaH_2PO_4, 0.5 $CaCl_2$

Recording ACSF contained (in mM): 119 NaCl, 26 $NaHCO_3$, 10 glucose, 2.5 KCl, 2.5 $CaCl_2$, 1.3 $MgCl_2$, 1 NaH_2PO_4

All ACSF was equilibrated with carbogen (95% O_2, 5% CO_2).

Potassium-gluconate based intracellular solution contained (in mM): 135 K-gluconate, 10 HEPES, 0.5 EGTA, 20 KCl, 2 MgATP, 5 phosphocreatine. Osmolarity: 300 mOsm. pH was adjusted to 7.2 with KOH.

Cesium based intracellular recording solution contained (in mM): 145 CsCl, 10 HEPES, 0.2 EGTA, 2 $MgCl_2$, 2 NaATP, 0.5 NaGTP, 5 phosphocreatine. Osmolarity: 305 mOsm. pH was adjusted to 7.2 with CsOH.

Potassium-chloride based intracellular recording solution contained (in mM): 145 KCl, 10 HEPES, 0.1 EGTA, 2 MgCl2, 2 Na2ATP. Osmolarity: 305 mOsm. pH was adjusted to 7.3 with KOH.

Drugs for electrophysiological recordings

All drugs were purchased from Tocris Bioscience, USA.

Primer for genotyping

Shank2 S1 forward: 5´ - TCC ATG GTT TCG GCA GAG CG - 3´

Shank2 AS1 reverse: 5´ - TCC CTA TTG GGA GGC AGT GG - 3´

Shank2 AS2 reverse: 5´ - CAG CAT CAT GAC AAT GTC TCC A - 3´

A polymerase chain reaction with DNA extracted from animal tail cuts will produce the following bands: A single band (299 base pairs (bp)) in homozygous *Shank2*$^{-/-}$, two bands (698 bp, 146 bp) in homozygous wildtypes, and three bands (698 bp, 299 bp, 146 bp) in heterozygous *Shank2*$^{+/-}$ animals.

Commercial reaction kits

DirectPCR®-Tail (Peqlab, Erlangen, Germany)

peqGold Proteinase K (Peqlab, Erlangen, Germany)

MangoTaq™ DNA Polymerase (Bioline, Luckenwalde, Germany)

2.2 Technical equipment

Vibratome VT 1200 (Leica, Wetzlar, Germany)

Amplifier Axoclamp 700a (Molecular Devices, Toronto, Canada)

Digitizer BNC 2090 (National Instruments, Austin, Texas, USA)

A/D Board PCI 6035E (National Instruments, Austin, Texas, USA)

Extracellular stimulation unit Iso Flex (A.M.P.I, Jerusalem, Israel)

Stimulus generator Master 8 (A.M.P.I, Jerusalem, Israel)

Oscilloscope HG-1507-3 (HAMEG Instruments, Mainhausen, Germany)

Glass electrode puller DMG Universal Puller (Zeitz-Instrumente, Munich, Germany)

Borosilicate glass capillaries, 1.5 mm outer diameter (Harvard Apparatus, Kent, UK)

Ag/AgCl electrode (Science products, Hofheim, Germany)

Bath electrode (Science products, Hofheim, Germany)

Upright microscopes (Olympus BX-51WI, equipped with Differential Interference Contrast (DIC) optics and video microscopy)

Olympus LumPlan FI 60x 0.9NA water immersion

Olympus UPlanFL N 4X×0.13 PhP

Mirror unit U-MWU2

Micromanipulators Mini 25, 3 axes (Luigs & Neuman, Ratingen, Germany)

Submerged recording chamber (Luigs & Neuman, Ratingen, Germany)

Plastic syringes (B. Braun, Melsungen, Germany)

Perfusion tubing (Carl Roth, Karlsruhe, Germany)

Software

IGOR Pro 4.0 (WaveMetrics Inc., OR, USA)

MATLAB 7.1 (The Mathworks Inc., USA)

Graph Pad Prism 5 (GraphPad Software, USA)

NeuroMatic (http://www.neuromatic.thinkrandom.com)

2.3 Animal handling and tissue preparation

Generation of the *ProSAP1/Shank2*$^{-/-}$ mice is described in detail in Schmeisser et al. (2012). In brief, a 16.3 kb chromosomal DNA fragment coding for exon VI and VII of the *Shank2* gene was cloned and a neomycin resistance gene flanked by loxP sites was inserted. This construct was introduced into embryonic stem cells of the mouse strain SC129/J and the selection cassette was deleted. Correctly targeted ES cells were microinjected into blastocytes of mouse strain C57BL/6. Heterozygous offsprings were backcrossed into mouse strain C57BL/6, allele excision

was performed by cross-breeding with transgenic mice expressing Cre under control of a CMV promotor. This resulted in total knockout mice.

Shank2$^{-/-}$ mice were raised on a C57BL/6J background using a heterozygous breeding protocol. All experiments including animals were performed according to the regulations of Berlin animal experiment authorities and the animal welfare committee of the Charité Berlin (File reference: T100/03). Wild-type littermates were used as a control in all experiments. Experimenters were blind to the genotype of the tested animals for data collection and analyses for all experiments involving extracellular fEPSP and intracellular mEPSC/mIPSC/sIPSC recordings.

DNA extraction from tail cuts, PCR for genotyping, and DNA gel electrophoresis were performed according to standard protocols (see for example Sambrook and Russel 2001) and, if involving commercially available enzymes and kits, followed the instructions of the supplier. Tail cuts were taken from pups at P10-P16; a second sample was taken for control purposes after sacrificing the animal.

Slice preparation

Hippocampal brain slices were prepared from animals of both sexes aged P21-P28 (unless indicated otherwise). Briefly, mice were anesthetized with isoflurane and decapitated. Brains were rapidly removed and transferred to ice-cold ACSF slicing solution. Tissue blocks containing the hippocampus were mounted on a Vibratome (Leica VT1200) and cut into horizontal slices of 300 µm. Slices were incubated submerged in slicing solution at 35°C for 30 min, transferred to recording ACSF (35 °C), and cooled to room temperature (RT). Slices were stored under submerged conditions for 30 min to 6 hours before being transferred to a submerged recording chamber where they were perfused with room-temperatured ACSF at a rate of 3-4 ml/min. All ACSF was equilibrated with carbogen (95% O_2, 5% CO_2).

2.4 Electrophysiological recordings and analyses

Recordings were performed with an Axopatch 700A Amplifier. Data were acquired using a BNC-2090 adapter chassis, digitized at 5 kHz, filtered at 1 or 2 kHz and recorded in IGOR Pro 4.0 using custom made plug-ins.

Extracellular field recordings

Stimulation and recording pipettes were pulled from borosilicate glass with a micropipette electrode puller. Evoked postsynaptic responses were induced by stimulating Schaffer collaterals in CA1 stratum radiatum with pipettes of ~ 20 µm tip diameter (filled with recording ACSF) using a stimulus isolator. Field excitatory postsynaptic potentials (fEPSPs) were recorded with the same pipettes that were placed in stratum radiatum. fEPSP slopes were determined as dV/dt of the 20 to 80 % amplitude from averages of five individual traces.

LTP was induced by a single tetanus of 100 pulses at 100 Hz. For LTD experiments, CA1 was

isolated by a microcut set at the border of CA2/CA3 immediately before the experiment and recordings were made in the presence of 1 µM gabazine. LTD was induced by 15 min paired pulse stimulation at 1 Hz with 50 ms between single pulses.

Whole-cell patch-clamp recordings

Pipettes had resistances of 2–3 MΩ. CA1 pyramidal cells were held in voltage-clamp mode at -60 mV unless noted otherwise. Liquid junction potential was not corrected. Series resistance (not compensated) was constantly monitored and was not allowed to increase beyond 22 MΩ or change more than 20 % during the experiment.

Miniature excitatory postsynaptic currents (mEPSCs) and whole-cell AMPA currents were recorded in the presence of 1 µM tetrodotoxin, 0.1 mM cyclothiazide, and 1 µM gabazine with a potassium-gluconate based intracellular recording solution. mEPSC events were detected with a threshold-based algorithm in NeuroMatic and their amplitudes were calculated from a 1 ms time window around the peak. Events were aligned by their rise time before averaging. The mEPSC frequency was determined from a 3 min time window. The analysis of mEPSC amplitudes includes the first 42 events of each recorded cell (one cell with fewer events was excluded from amplitude analysis). Cellular input resistance was calculated from the steady state current measured in response to a hyperpolarising command pulse (4 mV, 50 ms) at a holding potential of -60 mV.

Spontaneous and miniature inhibitory postsynaptic currents (sIPSCs and mIPSCs) were recorded in the presence of 10 µM NBQX and 10 µM APV with a potassium-chloride based intracellular recording solution. For mIPSC recordings, 1 µM tetrodotoxin was added to the bath. Frequency of events was determined from a 2 min time window. The analysis of sIPSC (mIPSC) amplitudes include the first 260 (120) events of each recorded cell.

In all experiments involving extracellular stimulation, single-peak EPSCs were evoked by stimulating Schaffer collaterals in CA1 stratum radiatum with pipettes of ~ 20 µm tip diameter (filled with recording ACSF) using a stimulus isolator.

AMPA/NMDA receptor ratios were recorded in ACSF containing 4 mM $CaCl_2$ and 4 mM $MgCl_2$ (condition A) or 2.5 mM $CaCl_2$ and 1.3 mM $MgCl_2$ (condition B). Experiments were performed in the presence of 1 µM gabazine with a cesium based intracellular recording solution. Compound EPSCs were evoked at –60 and +40 mV. Five to ten consecutive EPSCs for each holding potential were averaged. The AMPAR-mediated component of the EPSC was estimated by measuring the peak amplitude of the averaged EPSC at −60 mV. The NMDAR-mediated component was estimated at +40 mV by measuring the amplitude of the averaged EPSC 75 ms after stimulation. A/N ratios measured under one condition (A or B, respectively) were normalized to the median A/N ratio of the respective wildtype littermate control. In a cross-condition comparison separately performed for each genotype, normalized A/N ratios acquired under recording condition A and B were statistically indistinguishable (wildtype: median, 25th to 75th percentile for condition A: 1.00, 0.74 to 1.44; n(N) = 23(6), condition B: 1.00, 0.72 to

1.79; n(N) = 18(6); *Shank2*$^{-/-}$: median, 25th to 75th percentile for condition A: 0.70, 0.65 to 0.94; n(N) = 21(6); condition B: 0.62, 0.44 to 0.98; n(N) = 19(6); two-way ANOVA: p = 0.90). Thus, normalized A/N ratios acquired under condition A and condition B were pooled.

Minimal stimulation experiments were performed in the presence of 1µM gabazine with a cesium based intracellular recording solution. Stimulation was adjusted to produce a single-peak response, stimulation frequency was 0.2 Hz. At +40 mV holding potential, stimulation intensity was reduced until occasional transmission failures were observed (in ~ 5-20% of events), and 20-50 events were recorded at this stimulation intensity. Cells were subsequently clamped to -60 mV holding potential, and 30-50 events were recorded with the same stimulation intensity. In a subset of experiments, this order was reversed, i.e. stimulation intensity was adjusted and minEPSCs were recorded at -60 mV, before cells were clamped to +40 mV. We did not observe systematic differences in failure rates or amplitudes of minEPSCs between the two regimes. Experiments with systematically increasing or decreasing failure rates and/or minEPSC amplitudes at any holding potential were excluded from the analysis. Post-hoc analysis counted an NMDAR failure, whenever the EPSC charge (10 to 60 ms after stimulation) did not exceed the mean control charges of that experiment determined in two time windows (10 to 60 ms before as well as 190-240 ms after stimulation). The NMDAR miniature EPSC (minEPSC) amplitude was determined from a 5 ms window centered to 40 ms after stimulation. AMPAR failures were defined as events with a minEPSC peak smaller than four times the signal noise. The signal noise was defined as the mean SD of the signal in a 3 ms time window (the SD was averaged over all sweeps included into the analysis). Care was taken that the signal noise was not different between experimental groups; experiments with high background noise were excluded from the analysis. The time windows for signal noise detection and for minEPSC peak detection were located equidistant to the time window used for setting the baseline of the recorded sweep. The fraction of silent synapses was calculated from the failure rates determined for hyperpolarized and depolarized holding potentials (F_H and F_D, respectively) according to the following logic (Liao et al. 1995):

Under the assumptions that release probability of single quanta is low and that events are independent, synaptic transmission under minimal stimulation can be described by a Poisson distribution (del Castillo and Katz 1954)

$$P(k) = \frac{m^k e^{-m}}{k!}$$

with m being the average number of quanta released (the mean quantal content), e being euler‘s number, and P(k) being the probability that k quanta are released in a random experiment. For the analysis of transmission failures (k=0), this term simplifies to

$$P(0) = F = \frac{m^0 e^{-m}}{0!} = e^{-m}$$

with F being the failure rate of a given experiment.

This term can be converted to

$$m = ln\frac{1}{F} = -lnF \ .$$

We know that AMPAR-containing and AMPAR-lacking synapses contribue to EPSCs at +40 mV holding potential ($m_{A+ \cup A-}$), but only AMPAR-containing synapses are contributing to EPSCs at -60 mV holding potential (m_{A+}), thus

$$m_{A^+} = -lnF_H \qquad \text{and} \qquad m_{A^+ \cup A^-} = -lnF_D \ .$$

We are interested in the events mediated by silent synapses, i.e. synapses without AMPARs, which can be isolated as follows:

$$m_{A^-} = m_{A^+ \cup A^-} - m_{A^+}$$

or, after substitution with the terms above

$$m_{A^-} = -lnF_D - (-lnF_H) = -lnF_D + lnF_H \ .$$

Assuming that release is uniquantal, the quantal content equals the number of synapses N times release probability P_r:

$$m = NP_r \qquad \text{or} \qquad N = \frac{m}{P_r} \ .$$

Assuming equal release probabilites for all synapses, we can deduce that the fraction of silent synapses is equal to the fraction of their transmitted quanta:

$$\frac{N_{A^-}}{N_{A^- \cup A^+}} = \frac{\frac{m_{A^-}}{P_r}}{\frac{m_{A^- \cup A^+}}{P_r}} = \frac{m_{A^-}}{m_{A^- \cup A^+}}$$

We can thus calculate the average fraction of silent synapses from F_D and F_H as follows:

$$\frac{N_{A^-}}{N_{A^- \cup A^+}} = \frac{m_{A^-}}{m_{A^- \cup A^+}} = \frac{-lnF_D + lnF_H}{-lnF_D} = \frac{-lnF_D}{-lnF_D} + \frac{lnF_H}{-lnF_D} = 1 - \frac{lnF_H}{lnF_D}$$

Synaptic potency was defined as the mean minEPSC amplitude excluding failures (Stevens and Wang 1994), with AMPAR and NMDAR potency referring to minEPSC amplitudes recorded at -60 mV and +40 mV, respectively. The analysis of synaptic potency was performed on datasets with equal mean failure rates in wildtype and *Shank2*$^{-/-}$ mice. In the juvenile group (P13-P14) we excluded one experiment in wildtype mice with F_H < 20 %, such that mean failure rates in the resulting datasets were: F_H wildtype: 44.3 ± 19.6 %, F_H *Shank2*$^{-/-}$: 44.4 ± 20.6 %; F_D wildtype: 17.3 ± 6.8 %, F_D *Shank2*$^{-/-}$: 18.8 ± 8.3 %. In the adolescent group (P21-P28), we restricted the analysis to those experiments where 3 % < F_H < 40 %. After excluding one wildtype and five *Shank2*$^{-/-}$ experiments, the resulting dataset‘s mean failure rates were: F_H wildtype: 17.0 ± 10.4 %, F_H *Shank2*$^{-/-}$: 19.4 ± 12.5 %; F_D wildtype: 10.3 ± 7.6 %, F_D *Shank2*$^{-/-}$: 9.0 ±

3.8 %. We are aware that this probably leads us to underestimate the difference between genotypes concerning the AMPAR potency (as this resulted in the youngest *Shank2*$^{-/-}$ animals being excluded from the analysis). However, we preferred this conservative estimation over one which will certainly be overestimate the differences between genotypes. The coefficient of variation (CV) was calculated over the mean minEPSC amplitudes (excluding failures) of all experiments included in that analysis.

Statistics and data presentation

Analyses were performed using custom written procedures in IGOR Pro and MATLAB. Data in graphs and in the text are presented as mean ± sample standard deviation (SD). GraphPad Prism was used for statistical comparisons between groups and fitting of linear regressions. Unpaired two-tailed Student‘s t-test (short: Student‘s t-test) and two-way repeated measures ANOVA were used to compare normally distributed data. Non-parametric data was analysed by Mann-Whitney U test, Kruskal-Wallis with Dunn‘s post-test, and Dunn‘s multiple comparison test. The F test was used to test whether the slope of a linear regression was significantly non-zero. Two-sample Kolmogorov-Smirnov test (short: Kolmogorov-Smirnov test) was performed in MATLAB. Results were considered significant at $p < 0.05$. If Kolmogorov-Smirnov and t-test gave conflicting results, differences between datasets were classified as „trend“.

Stimulus artifacts were blanked or cropped in sample traces. Sample sizes are given as number of experiments (n) and number of animals (N). Data are presented as mean ± SD, circles in bar graphs show individual data points.

3 Results

3.1 Synaptic transmission is reduced in *Shank2*$^{-/-}$ mice

For a first characterization of synaptic transmission in *Shank2*$^{-/-}$ mice, we performed extracellular recordings of field excitatory postsynaptic potentials (fEPSPs) in the CA1 region of the hippocampus (Figure 8). We stimulated the CA3 Schaffer collaterals and compared the size of the presynaptic fibre volley (the presynaptic input) to the slope of the fEPSP (the postsynaptic output). Relative to wildtypes, *Shank2*$^{-/-}$ mice displayed a ~ 40 % decrease in basal synaptic transmission. This phenotype was evident in adolescent animals (3-4 weeks), as well as adults (3 month) (3-4 weeks: Figure 8a$_2$, wildtype: n(N) = 8(3), *Shank2*$^{-/-}$: n(N) = 11(4), repeated-measures ANOVA: $p < 0.05$; 3 month: Figure 8b; wildtype: n(N) = 7(3); *Shank2*$^{-/-}$: n(N) = 7(3), repeated measures ANOVA: $p < 0.05$). Heterozygous *Shank2*$^{+/-}$ mice displayed a similarly decreased input/output ratio (assessed in adolescent mice only, Figure 8a$_3$; wildtype: n(N) = 8(3), *Shank2*$^{+/-}$: n(N) = 11(3), repeated-measures ANOVA: $p < 0.05$). There was no evidence for genotypic differences in the excitability of the presynaptic fibres (Figure 8c; wildtype: n(N) = 27(6), *Shank2*$^{-/-}$: n(N) = 36(7), repeated measures ANOVA: $p = 0.34$).

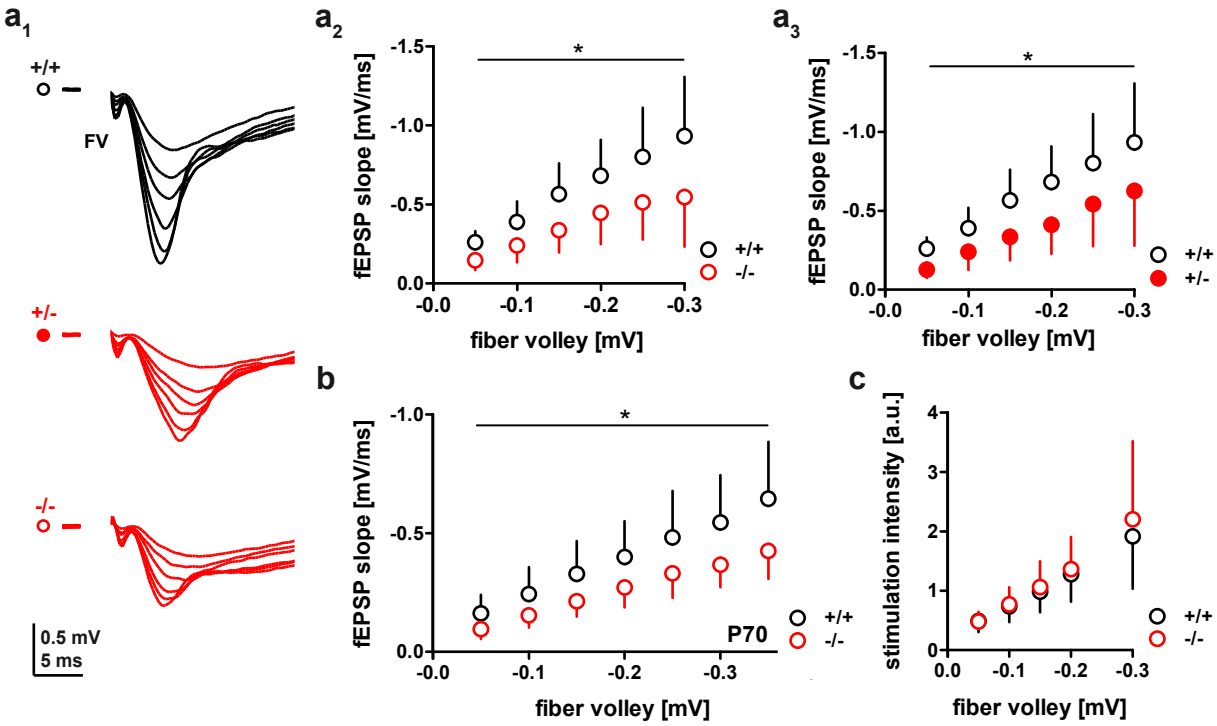

Figure 8. Reduced input/output ratio of CA1 fEPSPs in Shank2$^{-/-}$

a, b. Input/output ratio of CA1 fEPSPs. As illustrated in the sample traces (a$_1$), homozygous (a$_2$) as well as heterozygous (a$_3$) *Shank2* deficient mice suffer from reduced synaptic transmission at the age of P21-P28 (all genotypes were assessed in parallel; the wildtype data is replotted in a$_2$ and a$_3$). A reduced input/output ratio is also found in *Shank2*$^{-/-}$ mice at three month (b). **c**. The excitability of CA3 Schaffer collaterals is expressed as the electrical stimulation intensity that is needed to evoke a certain fibre volley amplitude. a.u.: arbitrary units. Data are presented as mean ± SD (standard deviation). Only one half of the SD error bar is shown for clarity. *: $p < 0.05$ (repeated measures ANOVA).

3.2 Reduced transmission selectively affects excitatory synapses

To test whether the reduced input/output ratio of fEPSPs was specific for excitatory synaptic transmission, we recorded spontaneous synaptic transmission from excitatory as well as inhibitory synapses of CA1 pyramidal cells. When we analysed miniature excitatory postsynaptic currents (mEPSCs) (Figure 9), *Shank2*$^{-/-}$ mice showed a ~ 30 % reduction in the frequency of mEPSC events (Figure 9b; wildtype: 0.62 ± 0.27 Hz, n(N) = 12(4), *Shank2*$^{-/-}$: 0.43 ± 0.21 Hz, n(N) = 16(5), Students t-test: $p < 0.05$). There was no evidence for differences between genotypes with respect to mEPSC amplitudes, neither in the comparison of mean values nor of the cumulative distribution of mEPSC amplitudes (Figure 9c; mean mEPSC amplitudes: wildtype: -12.9 ± 6.4 pA, n(N) = 12(4), *Shank2*$^{-/-}$: -12.6 ± 5.8 pA, n(N) = 16(5), Students t-test: $p = 0.37$; cumulative distribution of events: wildtype: 504 events, n(N) = 12(4), *Shank2*$^{-/-}$: 630 events, n(N) = 15(5), Kolmogorov-Smirnov test: $p = 0.96$).

Next we analysed spontaneous GABAergic synaptic transmission. Frequency and amplitude of inhibitory postsynaptic currents (IPSCs) onto CA1 pyramidal cells were largely unchanged in *Shank2*$^{-/-}$ mice (Figure 10). Specifically, there was no evidence for a genotypic difference in the frequency of miniature or spontaneous IPSCs (mIPSCs, sIPSCs) (Figure 10b; mIPSC frequency: wildtype: 5.0 ± 2.3 Hz, n(N) = 10(2), *Shank2*$^{-/-}$: 4.4 ± 2.1 Hz, n(N) = 13(2), Students t-test: $p = 0.53$; sIPSC frequency: wildtype: 5.5 ± 2.6 Hz, n(N) = 11(3), *Shank2*$^{-/-}$: 6.2 ± 3.2 Hz, n(N) = 11(3), Students t-test: $p = 0.73$). Concerning the amplitudes, we did observe a trend towards slightly lower mIPSC amplitudes in *Shank2*$^{-/-}$ mice. However, no such trend was evident from our recordings of sIPSCs (Figure 10c; mIPSCs: wildtype: -30.4 ± 4.2 pA, n(N) = 10(2), *Shank2*$^{-/-}$: -27.0 ± 4.7 pA, n(N) = 13(2), Students t-test: $p = 0.08$, Kolmogorov-Smirnov test:

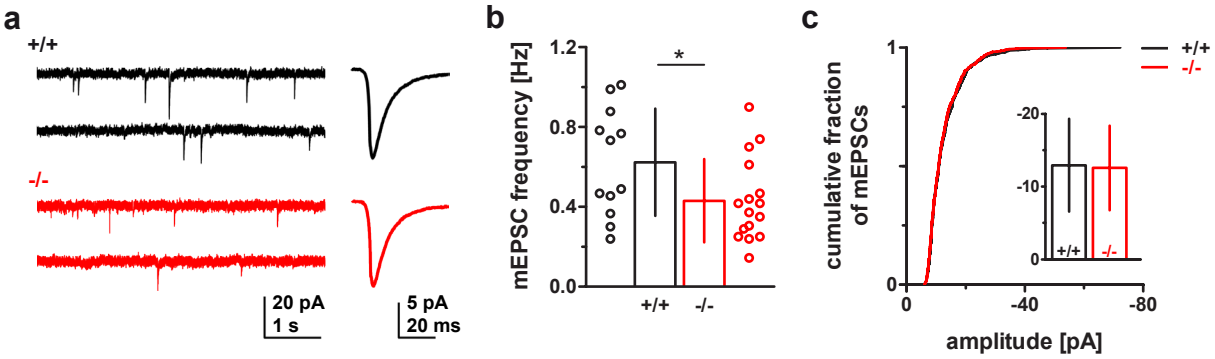

Figure 9. mEPSC frequency, but not amplitude is decreased in Shank2$^{-/-}$

a. Sample traces of individual recordings (left), averages of all mEPSC events (right). **b.** mEPSC frequency is reduced in *Shank2*$^{-/-}$. **c.** mEPSC amplitudes plotted as cumulative distribution and mean cellular mEPSC amplitudes (inset). Bars represent mean ± SD. *: $p < 0.05$ (Students t-test).

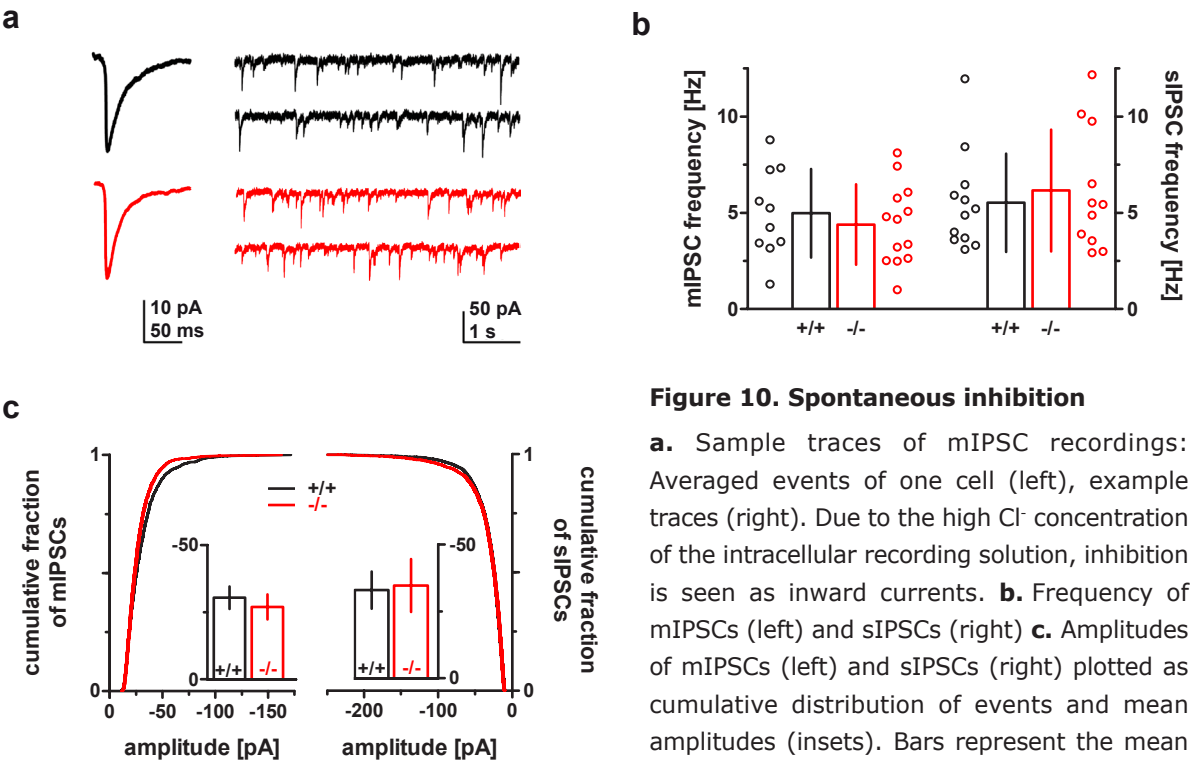

Figure 10. Spontaneous inhibition

a. Sample traces of mIPSC recordings: Averaged events of one cell (left), example traces (right). Due to the high Cl^- concentration of the intracellular recording solution, inhibition is seen as inward currents. **b.** Frequency of mIPSCs (left) and sIPSCs (right) **c.** Amplitudes of mIPSCs (left) and sIPSCs (right) plotted as cumulative distribution of events and mean amplitudes (insets). Bars represent the mean ± SD.

$p < 0.05$ (wildtype: 1200 events, *Shank2*$^{-/-}$: 1560 events); sIPSCs: wildtype: -32.9 ± 7.0 pA, n(N) = 11(3), *Shank2*$^{-/-}$: -34.6 ± 9.9 pA, n(N) = 11(3), Students t-test: $p = 0.65$, Kolmogorov-Smirnov test: $p = 0.37$ (wildtype: 2860 events, *Shank2*$^{-/-}$: 2860 events)).

3.3 General properties of pyramidal cells in *Shank2*$^{-/-}$ mice

In a next step, we analysed general properties of CA1 pyramidal cells in *Shank2*$^{-/-}$ mice (Figure 11). The intrinsic firing threshold was estimated from CA1 field recordings. It was defined as the fEPSP slope at which the CA1 population spike first became visible as a contamination of fEPSP decay kinetics. Based on this analysis, we did not find evidence for a change in firing threshold between genotypes (Figure 11a; wildtype: -0.41 ± 0.16 mV/ms, n(N) = 25(6), *Shank2*$^{-/-}$: -0.40 ± 0.20 mV/ms, n(N) = 36(7)), Students t-test: $p = 0.87$). Whole-cell patch-clamp recordings did not reveal evidence for a genotypic difference in the cellular input resistance of CA1 pyramidal cells (Figure 11b; wildtype: 268 ± 91 MΩ, n(N) = 16(3), *Shank2*$^{-/-}$: 282 ± 80 MΩ, n(N) = 17(5), Students t-test: $p = 0.92$). When we stimulated the Schaffer collaterals to evoke excitatory postsynaptic currents (EPSCs), we did not find evidence for differences in the EPSC paired pulse ratio (100 ms inter pulse interval; Figure 11c; wildtype: 1.36 ± 0.12, n(N) = 26(8), *Shank2*$^{-/-}$: 1.37 ± 0.17, n(N) = 26(7), Students t-test: $p = 0.78$). We also compared the surface AMPA receptors (synaptic + extrasynaptic) by measuring the whole-cell

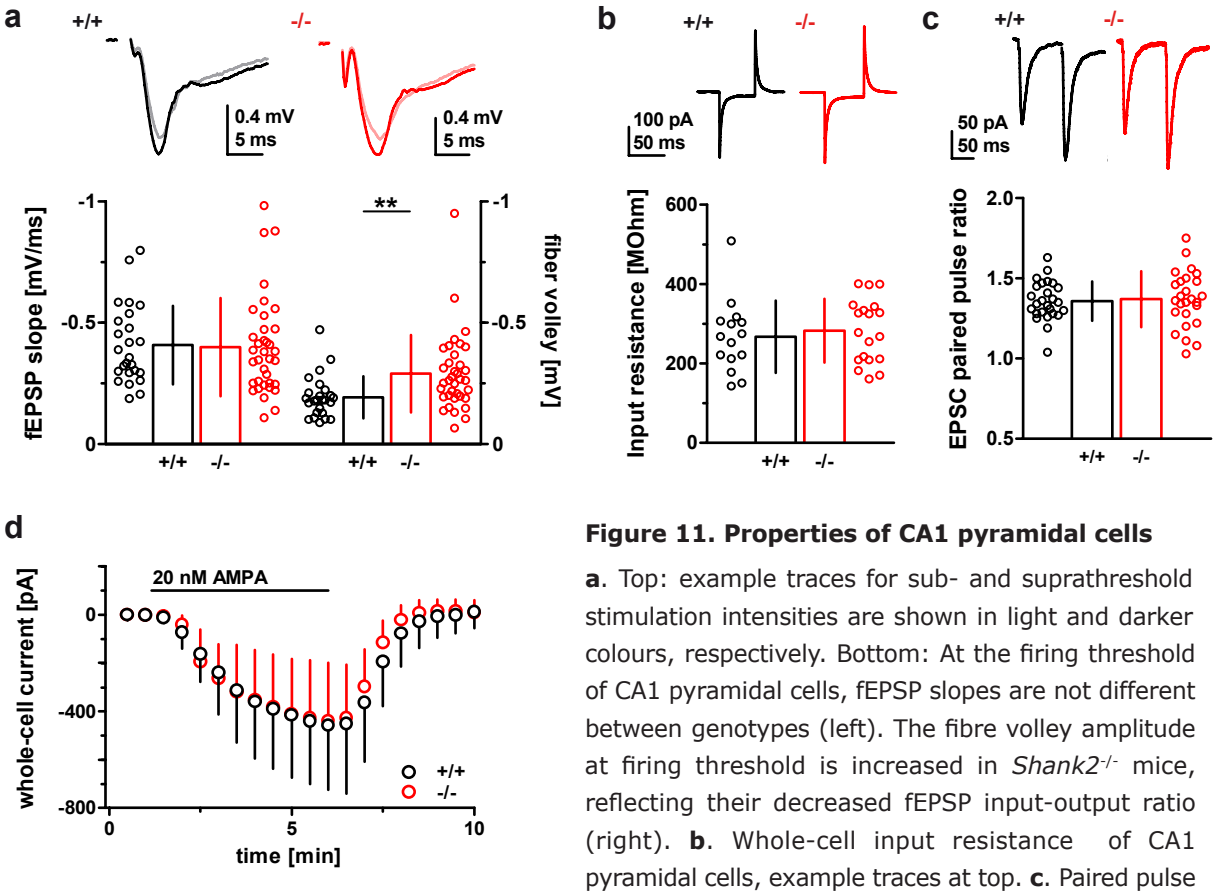

Figure 11. Properties of CA1 pyramidal cells

a. Top: example traces for sub- and suprathreshold stimulation intensities are shown in light and darker colours, respectively. Bottom: At the firing threshold of CA1 pyramidal cells, fEPSP slopes are not different between genotypes (left). The fibre volley amplitude at firing threshold is increased in *Shank2*$^{-/-}$ mice, reflecting their decreased fEPSP input-output ratio (right). **b**. Whole-cell input resistance of CA1 pyramidal cells, example traces at top. **c**. Paired pulse ratio of EPSCs evoked by Schaffer collateral stimulation (100 ms interpulse interval), example traces at top. **d**. Whole-cell currents evoked by bath application of 20 nM AMPA (only one half of the SD error bar is shown for clarity). Data are presented as mean ± SD. **: $p < 0.01$ (Students t-test).

current evoked by bath application of 20 nM AMPA. We found no evidence for differences between genotypes (Figure 11d; wildtype: -455 ± 268 pA, n(N) = 8(3), *Shank2*$^{-/-}$: -434 ± 233 pA, n(N) = 9(3), Students t-test: $p = 0.9$).

3.4 Synaptic plasticity in *Shank2*$^{-/-}$ mice

We further analysed synaptic long-term plasticity in *Shank2*$^{-/-}$ mice in CA1 field recordings (Figure 12). NMDAR-dependent long-term potentiation (LTP) was induced by high frequency stimulation of the Schaffer collaterals (100 pulses at 100 Hz), a protocol that reliably induced LTP. We monitored fEPSP for 30 minutes after LTP induction; at that time point, potentiation was slightly but significantly enhanced in *Shank2*$^{-/-}$ compared to wildtype mice (Figure 12a; potentiation 30 min after induction: wildtype: 38 ± 17 %, n(N) = 30(5), *Shank2*$^{-/-}$: 56 ± 20 %, n(N) = 34(6), Students t-test: $p < 0.001$). Long-term depression (LTD) was induced by paired

pulse low frequency stimulation; we did not obtain evidence for differences between genotypes with this protocol (Figure 12b; depression 40 min after induction: wildtype: 23 ± 13 %, n(N) = 5(2), *Shank2*$^{-/-}$: 26 ± 9 %, n(N) = 6(2), Students t-test: p = 0.72).

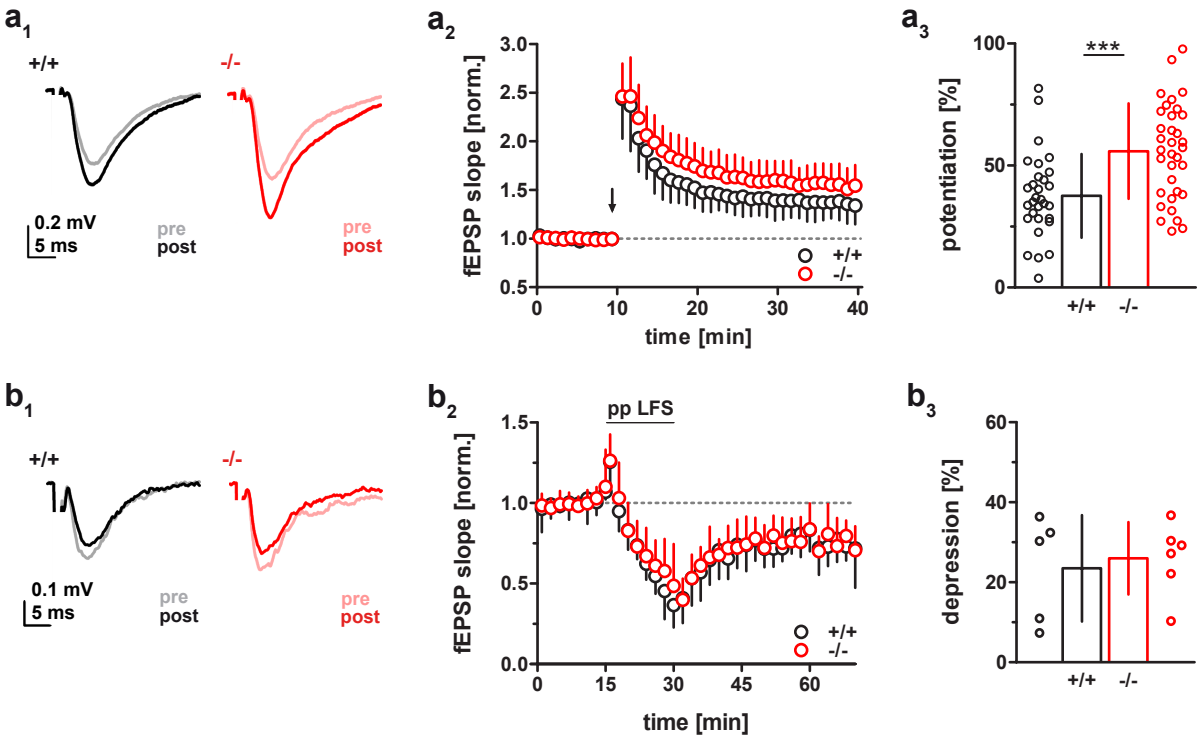

Figure 12. Synaptic long-term plasticity

a. LTP is increased in *Shank2*$^{-/-}$ mice, as evident from the sample traces (a_1), the average time plot of all recordings (a_2), and the ratio of fEPSP slopes 30 min after vs. before LTP induction (a_3). **b.** No evidence for genotypic differences in LTD. b_1. Example traces. b_2. Average time plot of all recordings. b_3. Depression of fEPSP slopes 40 min after vs. before LTD induction. Arrow: LTP induction (100 pulses at 100 Hz). pp LFS: LTD induction (paired pulse stimulation: 15 min, 1 Hz, 50 ms inter pulse interval). Data are presented as mean ± SD. In a_2 and b_2, only one half of the S.D. error bar is shown for clarity. ***: p < 0.001 (Students t-test).

3.5 AMPA/NMDA receptor ratios are decreased in *Shank2*$^{-/-}$ mice

In a next step, we compared the relative contribution of AMPA vs. NMDA receptors to evoked EPSCs in CA1 pyramidal cells. To this end, we stimulated the Schaffer collaterals and recorded the evoked EPSCs at different holding potentials. At -60 mV membrane potential, the NMDAR channel pore is blocked by Mg^{2+} and the recorded EPSC is mainly mediated by AMPARs. At +40 mV, the magnesium block is released from the NMDAR, and a compound EPSC mediated by NMDARs and AMPARs can be measured. To minimize the contribution of AMPAR currents, we determined the amplitude of the NMDAR EPSC 75 ms after stimulation, when the AMPAR component of the EPSC is decayed to (near) zero.

Over the course of the project, AMPA/NMDA receptor ratios (A/N ratios) were repeatedly measured under different recording conditions. Although the absolute values depended on the external conditions, these had no influence on data distribution or relative differences between genotypes. Thus, A/N ratios for each recording condition were normalized to the median A/N ratio of the respective wildtype littermate control and datasets were pooled (see methods for details). When we compared the normalized A/N ratios between genotypes, we found a ~ 30 % reduced A/N ratio in *Shank2*$^{-/-}$ vs. wildtype mice aged P21 to P28 (Figure 13; median, 25th to 75th percentile for wildtype: 1, 0.73 to 1.58, n(N) = 41(12); *Shank2*$^{-/-}$: 0.69, 0.50 to 0.93, n(N) = 40(12); Mann Whitney U test: $p < 0.001$).

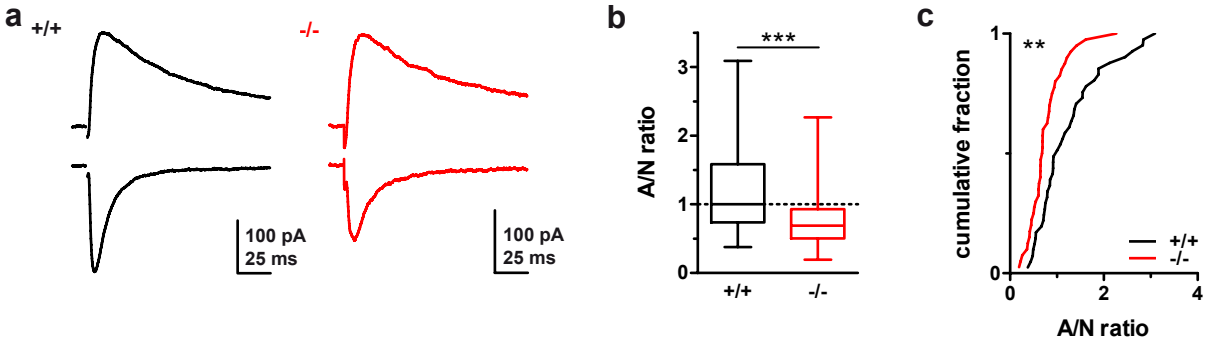

Figure 13. Decreased A/N ratio in Shank2$^{-/-}$

a. Example recordings of EPSCs evoked at +40 and -60 mV holding potential. **b.** Box plot of A/N ratios shows the median (horizontal line), the lower and upper quartiles (box boundaries), as well as the minimum and maximum (whiskers). **c.** Cumulative distribution of A/N ratios. All A/N ratios are normalized to the median value of the wildtype control (see text). **: $p < 0.01$ (Kolmogorov-Smirnov test), ***: $p < 0.001$ (Mann-Whitney U test).

3.6 The AMPA/NMDA receptor ratio is developmentally regulated

In a post-hoc data analysis (Figure 14a), we found A/N ratios to increase linearly over the course of the fourth postnatal week in wildtype animals. Due to the biologically high variance of A/N ratios, the correlation of the wildtype data with a linear fit was weak ($r^2 = 0.13$), but the slope was significantly different from zero (0.11 ± 0.05, F-test: $p < 0.05$) (Figure 14a$_1$). In *Shank2*$^{-/-}$ mice, the data/fit correlation was weaker ($r^2 = 0.09$) and the fitted slope was not significantly different from zero (0.04 ± 0.02, F-test: $p = 0.06$) (Figure 14a$_2$). Consequently, when the data was grouped according to animal age (P21-P24 vs. P25-P29), we found significant differences between genotypes in the second half of the 4th postnatal week, but not in the first (Figure 14a$_3$; P21-P24: median, 25th to 75th percentile for widltype: 0.86, 0.53 to 1.24; n(N) = 20(6); *Shank2*$^{-/-}$: 0.65, 0.42 to 0.82; n(N) = 22(7); Dunn's Multiple Comparison

Test: $p > 0.05$; P25-P29: median, 25th to 75th percentile for wildtype: 1.55, 0.85 to 2.01, n(N) = 21(6); *Shank2*$^{-/-}$: 0.81, 0.62 to 1.24, n(N) = 18(5); Dunn's Multiple Comparison Test: $p < 0.05$).

This prompted us to test the hypothesis that (1) A/N ratios in the CA1 region of the hippocampus show a significant increase during the 4th postnatal week in wildtype mice, and (2) that *Shank2*$^{-/-}$ mice are defective in this aspect of synaptic maturation. To this end, we recorded A/N ratios over a wider range of ages (P13-P14 and P21-P28) and did so by performing minimal stimulation, which would allow us to extract further information from those experiments (see below). Stimulation strength was decreased until occasional transmission failures occured and single unit EPSCs could be resolved; the A/N ratio was calculated from averages of 20 - 50 stimulations at each holding potential. As expected, we found that over the course of the fourth postnatal week, A/N ratios recorded with minimal stimulation showed a linear increase in the fourth postnatal week in wildtype mice, but not *Shank2*$^{-/-}$ mice (wildtype: Figure 14b$_1$, $r^2 = 0.52$, F-test: $p < 0.001$; *Shank2*$^{-/-}$: Figure 14b$_2$, $r^2 = 0.02$, F-test: $p = 0.56$). Interestingly, the increase of A/N ratios in wildtype mice was more prominent from P21-P24 to P25-P28 than the increase from P13-P14 to P21-P24. Thus, significant differences between the A/N ratios of *Shank2*$^{-/-}$ and wildtype mice were again found selectively in the age group of P25-P28 (Figure 14b$_3$; P25-P28:

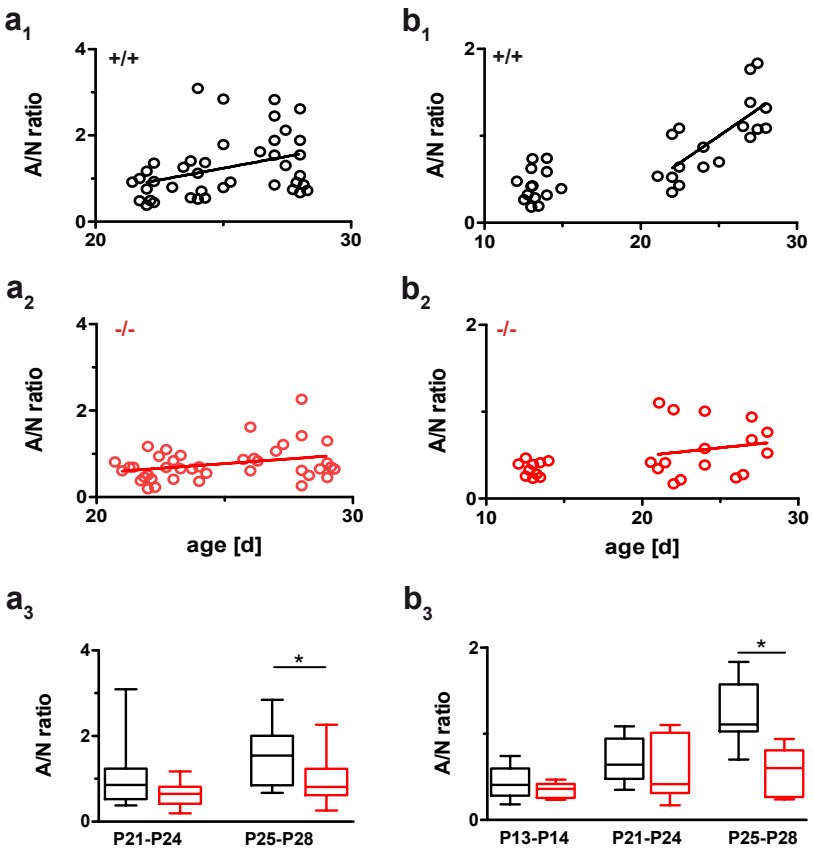

Figure 14. Maturation of the A/N ratio is attenuated in Shank2$^{-/-}$

A/N ratios estimated from (a) normal and (b) minimal stimulation increase during postnatal development in wildtype mice (a_1, b_1). The attenuated A/N ratio maturation in *Shank2*$^{-/-}$ mice (a_2, b_2) results in significant differences between genotypes at P25-P28 (a_3, b_3). Box plots show the median (horizontal line), the lower and upper quartiles (box boundaries), as well as the minimum and maximum (whiskers). A/N ratios are normalized to the median value of the wildtype control (P21-P28). *: $p < 0.05$ (Kruskal Wallis with Dunn's post-test).

median, 25th to 75th percentile for wildtype: 1.11, 1.03 to 1.58, n(N) = 9(3); *Shank2*$^{-/-}$: 0.60, 0.27 to 0.81, n(N) = 6(3); Dunn's Multiple Comparison Test: $p < 0.05$; for easier comparison with the previous datasets, A/N ratios derived from minimal stimulation were also normalized to the median A/N ratio of all experiments in wildtype mice aged P21-P28).

3.7 Unsilencing of synapses is attenuated in *Shank2*$^{-/-}$ mice

A developmental increase in the A/N ratio is generally attributed to an increasing number of AMPA receptors being incorporated into the postsynaptic membrane. We hypothesized that the lack of progressive increase of the A/N ratio in *Shank2*$^{-/-}$ mice could stem from defective synapse maturation. To gain information about the properties of single synapses in *Shank2*$^{-/-}$ mice, we obtained EPSCs from minimal stimulation experiments. These minEPSCs allow conclusions on the strength of single synapses with respect to their AMPA and NMDA receptor signalling, as well as the fraction of AMPAR-silent synapses. This fraction is proportional to δF, the difference in the minEPSC failure rate recorded at hyperpolarized vs. depolarized potentials ($\delta F = F_H - F_D$).

At the end of the second postnatal week (P13-P14), wildtype mice on average showed a ~ 30 % higher failure rate at hyperpolarized than at depolarized potentials. From this we can estimate that at this age every second synapse is AMPAR-silent. Similar values were obtained

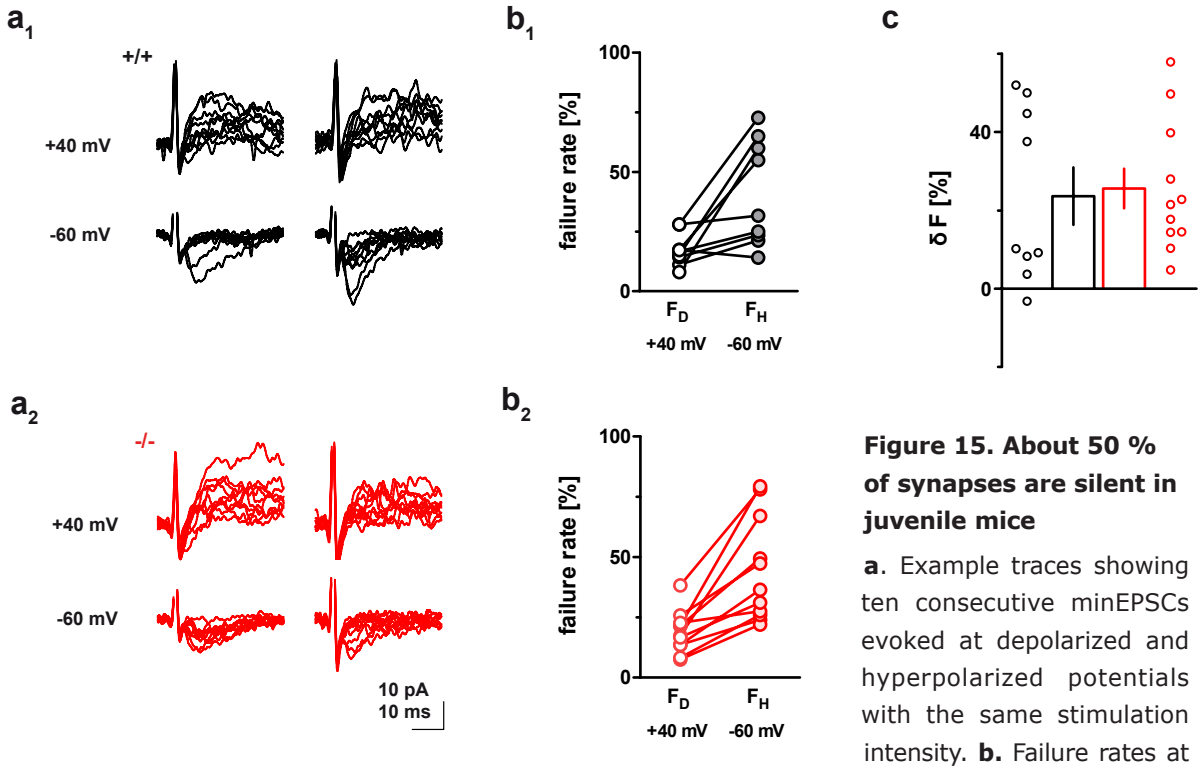

Figure 15. About 50 % of synapses are silent in juvenile mice

a. Example traces showing ten consecutive minEPSCs evoked at depolarized and hyperpolarized potentials with the same stimulation intensity. **b.** Failure rates at depolarized vs. hyperpolarized potentials (F_D vs. F_H) are plotted for each experiment. **c**. δF (= F_H- F_D) is represented as mean ± SD. No gross differences are obvious between genotypes.

for *Shank2*$^{-/-}$ mice (Figure 15; δF wildtype: 23.6 ± 22.0 %, n(N)=9(4), δF *Shank2*$^{-/-}$: 25.6 ± 16.8 %, n(N)=11(4), Students t-test: p = 0.82; silent synapses wildtype: 49 %, silent synapses *Shank2*$^{-/-}$: 51 %; see methods for details on silent synapse estimation).

At P21-P28, δF has become smaller in wildtypes, whereas it remains at a high level in *Shank2*$^{-/-}$ mice (Figure 16; δF: wildtype: 5.1 ± 10.3 %, n(N)=12(5), *Shank2*$^{-/-}$: 22.2 ± 19.2 %, n(N)=13(7), Students t-test: p < 0.05). Consequently, the fraction of silent synapses in the fourth postnatal week has dropped to 17 % in wildtypes, whereas it is still estimated to be 51 % in *Shank2*$^{-/-}$ mice.

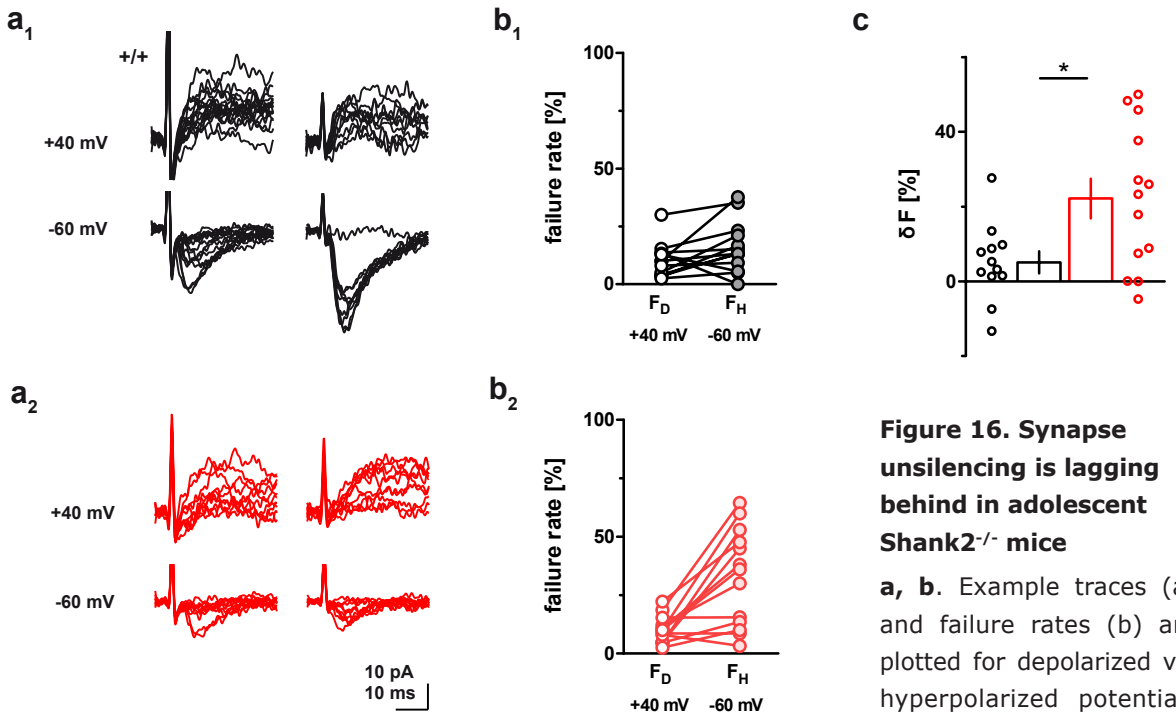

Figure 16. Synapse unsilencing is lagging behind in adolescent Shank2$^{-/-}$ mice

a, b. Example traces (a) and failure rates (b) are plotted for depolarized vs. hyperpolarized potentials for wildtype and *Shank2*$^{-/-}$ mice aged P21-P28. **c**. At that age, δF is significantly different between genotypes. Bars represent mean ± SD. *: p < 0.05 (Student's t-test).

3.8 Synaptic potency is misregulated in *Shank2*$^{-/-}$ mice

We also quantified the amplitude of non-failure minEPSCs recorded at +40 mV and -60 mV to learn about the potency conveyed to synapses by NMDA and AMPA receptors. As we adjusted the failure rate to be ~ 20 % at depolarized potentials, our minimal stimulation is likely to evoke simultaneous release from more than one synapse occasionally. To not confound our analysis by systematic variations in the number of signalling synapses (and thus the number of synapses contributing to one minEPSC), we restricted the amplitude analysis to a group of experiments with similar failure rates on average in both genotypes (see Materials and Methods for details).

Shank2$^{-/-}$ mice showed a trend towards slightly increased NMDAR amplitudes at juvenile stages (Figure 17; NMDAR potency in P13-P14: wildtype: 10.1 ± 3.0 pA, n(N) = 8(4), *Shank2*$^{-/-}$: 12.0 ± 4.3 pA, n(N) = 11(4), Students t-test: p = 0.32; Kolmogorov-Smirnov test: p < 0.001, n = 139 bins). However, in adolescent stages there was no evidence for differences between genotypes (P21-P28: wildtype: 8.7 ± 2.6 pA, n(N) = 11(5), *Shank2*$^{-/-}$: 9.2 ± 1.8 pA, n(N) = 8(6), Students t-test: p = 0.67; Kolmogorov-Smirnov test: p = 0.30, n = 140 bins). As the amplitudes measured at the soma are influenced by dendritic cable properties, and membrane properties are significantly different in juvenile vs. adolescent mice, we did not compare amplitudes quantitatively across age groups (input resistance at +40 mV holding potential for P13-P14: 133 ± 17 MΩ, n(N) = 20(8); P21-P28: 100 ± 20 MΩ; n(N) = 25(12); Students t-test: p < 0.001; genotypes pooled). We also noted that the coefficient of variation

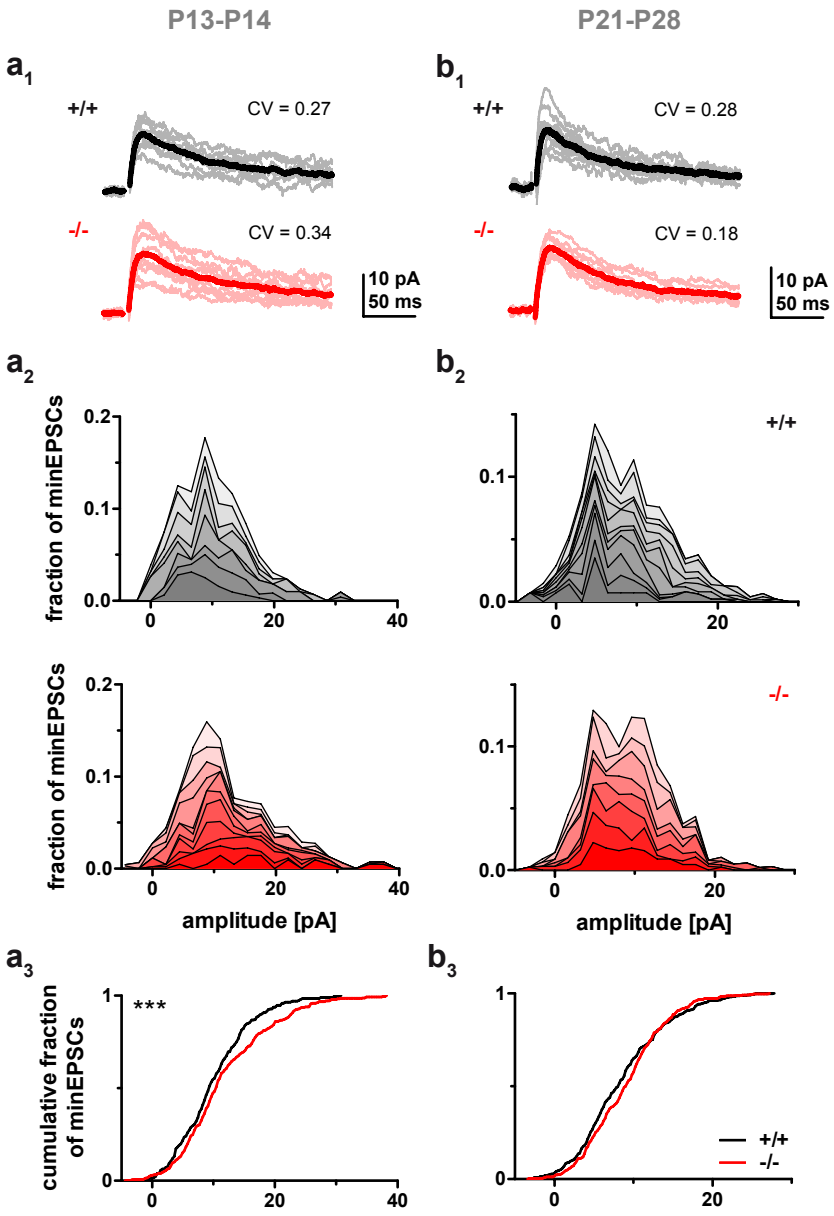

Figure 17. NMDAR potency is increased in juvenile *Shank2*$^{-/-}$ mice

NMDAR potency was determined from minEPSC amplitudes (excluding failures) in juvenile (a) and adolescent mice (b). **a$_1$, b$_1$**. Thin and bold lines represent average minEPSC of each experiment (excluding failures) and global average, respectively. Note the large coefficient of variation (CV) in juvenile *Shank2*$^{-/-}$ mice. **a$_2$, b$_2$**. Cumulative histograms of minEPSC amplitudes (excluding failures). The area between two lines represents the amplitudes of a single experiment, as histograms of individual recordings are plotted cumulatively. Areas are normalized for comparison. **a$_3$, b$_3$**. Cumulative distribution of NMDAR minEPSC amplitudes reveals differences in the NMDAR potency between genotypes in juvenile mice (a$_3$). ***: p < 0.001 (Kolmogorov-Smirnov test).

(CV) of minEPSC amplitudes did not change across age groups in wildtype, but did so in *Shank2*$^{-/-}$ mice, being higher than wildtype controls in juvenile and lower than wildtype controls in adolescent stages (Figure 17a$_1$, b$_1$).

Different observations were made for AMPAR minEPSC amplitudes. In juvenile *Shank2*$^{-/-}$ mice (P13-P14, Figure 18a), a decreased AMPAR potency in comparison to wildtype mice was apparent as a significant difference in the distribution of minEPSC amplitudes (Kolmogorov-Smirnov test: $p < 0.05$, n = 142 bins), and as a trend in the mean values (AMPAR potency in wildtype P13-P14: -13.2 ± 2.4 pA, n(N) = 8(4), *Shank2*$^{-/-}$ P13-P14: -11.7 ± 2.2 pA, n(N) = 11(4), Students t-test: $p = 0.18$). In adolescent *Shank2*$^{-/-}$ mice (P21-P28, Figure 18b), minEPSC amplitudes were significantly decreased in the cumulative distribution (Kolmogorov-Smirnov test: $p < 0.001$, n = 192 bins); the mean EPSC amplitudes did not reach significance, however (AMPAR potency in wildtype P21-P28: -20.0 ± 9.7 pA, n(N) = 11(5), *Shank2*$^{-/-}$ P21-P28:

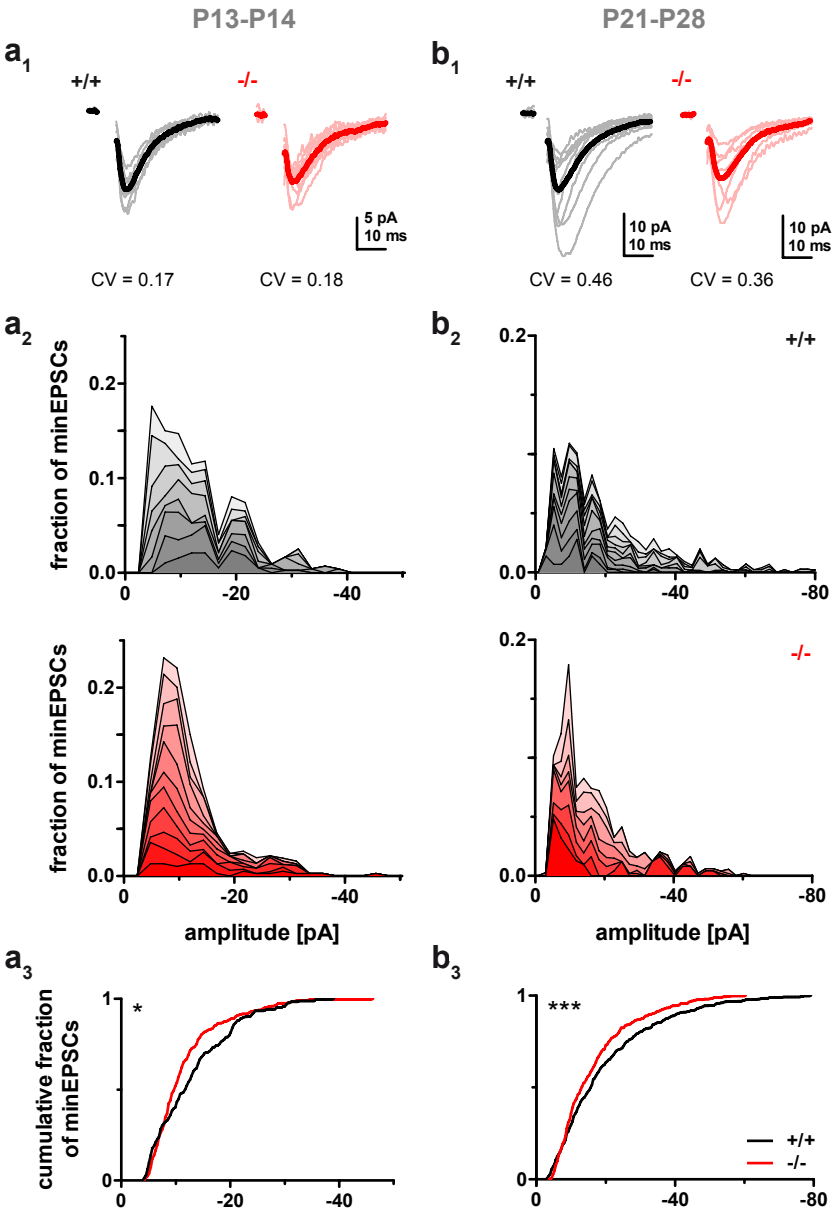

Figure 18. AMPAR potency is decreased in Shank2$^{-/-}$ mice

AMPAR potency in juvenile (a) and adolescent mice (b). **a$_1$, b$_1$**. Thin lines show the average AMPAR minEPSC (excluding failures) of each experiment. After averaging, traces were rise-time aligned for display and calculation of the global average (bold line). The coefficient of variation (CV) is similar for both genotypes and increases with age. **a$_2$, b$_2$**. Cumulative histograms of minEPSC AMPAR amplitudes (excluding failures). The area between two lines represents the AMPAR amplitudes of a single experiment, as histograms of individual recordings are plotted cumulatively. Areas are normalized for comparison. **a$_3$, b$_3$**. Cumulative distributions of minEPSC amplitudes reveal progressive differences in the AMPAR potency between genotypes. *: $p < 0.05$, ***: $p < 0.001$ (Kolmogorov-Smirnov test).

-16.8 ± 6.5 pA, n(N) = 8(6), Students t-test: p = 0.42). The coefficient of variation of minEPSC amplitudes was similar for *Shank2*$^{-/-}$ and wildtype mice and strongly increased with age (Figure 18a$_1$, b$_1$). Again, we did not perform a quantitative comparison of minEPSC amplitudes across age groups due to different input resistances in juvenile vs. adolescent mice (input resistance at -60 mV holding potential for P13-P14: 542 ± 166 MΩ, n(N) = 20(8); P21-P28: 274 ± 64 MΩ; n(N) = 25(12); Students t-test: p < 0.001; genotypes pooled).

4 Discussion

This thesis describes the first electrophysiological characterization of a transgenic mouse line deficient for the *Shank2* gene. We found that *Shank2*$^{-/-}$ mice suffer from attenuated synaptic maturation and decreased excitatory synaptic transmission in hippocampal CA1. Specifically, CA1 pyramidal cells of adolescent *Shank2*$^{-/-}$ mice harbour an unusually high fraction of silent synapses. Those synapses containing AMPARs have a reduced AMPAR potency. In consequence, the AMPAR vs. NMDAR ratio (A/N ratio) in *Shank2*$^{-/-}$ mice is lower than in wildtype controls, a difference that becomes manifest in the course of the third and fourth postnatal week. In accordance with *Shank2*$^{-/-}$ mice having fewer AMPAR-containing synapses, we observed a reduced frequency of mEPSCs in CA1 pyramidal cells and reduced synaptic transmission in extracellular field recordings. Knockout mice were, however, capable of long-term plasticity: They performed like wildtype mice after a paired pulse low frequency LTD protocol and showed increased LTP after tetanic stimulation.

To our knowledge, the work described in this thesis is the first electrophysiological quantification of silent synapses in the juvenile and adolescent hippocampus; we will thus start the discussion by comparing our electrophysiological results to data from earlier electron microscopy (EM) studies (chapter 4.1). We will further present some hypotheses on the role of Shank2 in synapse maturation (chapter 4.2). In chapter 4.3, we will outline agreements and discrepancies with studies of other research groups. We will close the discussion with our current view on the role of Shank proteins in neuronal physiology seen in the light of our study.

4.1 Synaptic maturation in adolescent rodents

The existence of functionally silent (that is: AMPAR-lacking) glutamatergic synapses in the hippocampus has been suggested almost twenty years ago (Kullmann 1994). A series of electrophysiological studies showed that AMPAR signalling in these synapses can be induced by NMDAR activation (Isaac et al. 1995, Liao et al. 1995, Durand et al. 1996), and evidence for the physical absence of AMPARs in Schaffer collateral synapses onto CA1 pyramidal cells has been presented in a number of EM studies (Nusser et al. 1998, Petralia et al. 1999, Takumi et al. 1999, Racca et al. 2000). It has been shown that the maturation of the hippocampal circuitry involves an increase in the A/N ratio (Hsia et al. 1998) and a decrease in the fraction of morphologically silent synapses (Liao et al. 1999). Electrophysiological studies on the developmental properties of synapses with minimal stimulation have been undertaken for thalamocortical connections (Isaac et al. 1997), and in the olfactory cortex (Franks and Isaacson 2005). For synapse maturation in the rodent hippocampus, EM studies invite the following predicitions: In adults (5 weeks), the fraction of silent synapses should be low (~ 14%), and the distribution of

AMPARs per synapse skewed towards higher values (Nusser et al. 1998). At that age, synapses should also display a high degree of heterogeneity in the number of AMPA, but not NMDA receptors (Takumi et al. 1999, Racca et al. 2000). Silent synapses should be more abundant in young animals (P10: ~ 49 %) and decrease with age (P17: ~ 28%) (Petralia et al. 1999). All these predicitions are met by our electrophysiological observations in wildtype mice: The fraction of silent synapses decreases from ~ 49 % at P13-P14 to ~ 17 % at P21-P28. In adolescent mice (P21-P28), the observed variation of AMPAR potency is much higher than the variation of NMDAR potency, and the histogram of AMPAR amplitudes is skewed towards higher values. Our study design does not allow a quantitative comparison of amplitudes across ages, as dendritic attenuation of minEPSCs is increasing substantially during development. However, we do observe an increase in the A/N ratio and in the variation of AMPAR potency with animal age. This corresponds well to the notion that network maturation in hippocampal CA1 involves the selective AMPAR-mediated strengthening of certain synapses, a process that leads to a progressive increase in synapse heterogeneity. We conclude that our experimental design is sufficient to describe synaptic properties of CA1 pyramidal cells, despite the problems associated with minimal stimulation (i.e. insufficient control over the precise number of synapses recruited) and somatic recordings of synaptic currents (i.e. signal attenuation due to dendritic filtering). Thus we are confident to say that in our recording conditions, adolescent *Shank2*$^{-/-}$ mice show strong defects in synaptic maturation, evident from (1) a reduced A/N ratio and (2) an increased fraction of silent synapses.

4.2 The role of Shank2 in synapse maturation and maintenance

The observation of insufficiently matured synapses in mice lacking Shank2 raises the question as to which neuronal processes are disturbed in the absence of this scaffold protein. Do we have - either from our data or from the data of others - indications to suggest a selective disturbance in the induction, the establishment, and/or the maintenance of mature synaptic connections in *Shank2*$^{-/-}$ mice? Shank2 is a scaffolding protein that directly and indirectly interacts with a multitude of partners in the PSD. It holds a strategic position suited to spatially and functionally integrate and coordinate a large set of cellular functions and signalling pathways. Some of these interactions might be of particular importance for synaptic maturation and/or synapse integrity; these interactions and their possible implications will be outlined in the following part of the discussion.

4.2.1 Synaptic AMPAR insertion

Compared to wildtypes, *Shank2*$^{-/-}$ mice lack the functional synaptic heterogeneity that is characteristic for the mature hippocampal CA1 circuit (Nusser et al. 1998). We have observed that the fraction of AMPAR containing synapses is decreased and AMPAR potency is reduced in adolescent *Shank2*$^{-/-}$ mice. Could it be the actual AMPAR insertion into the membrane or their anchoring at the PSD that is disturbed? Shank2 has been shown to interact with the cytoplasmic tail of GluA1 (Uchino et al. 2006), an interaction that could possibly be involved in AMPAR trafficking. It has been shown that GluA1-containing AMPARs are incorporated into synapses upon LTP induction (Shi et al. 1999, Hayashi et al. 2000) and that overexpression of a GluA1 subunit with a mutated PDZ-binding motif paradoxically decreases synaptic transmission after LTP induction to levels below baseline, supposedly via interference with constitutive AMPAR cycling (Hayashi et al. 2000). If synapse unsilencing and strengthening could not be efficiently manifested in *Shank2*$^{-/-}$ mice because AMPAR insertion into synapses was inefficient or mislocalized, this would explain a wide range of our findings. This hypothesis is, however, questioned by the fact that LTP in *Shank2*$^{-/-}$ mice is intact. Deficits in LTP expression after high-frequency stimulation and reduced GluA1 insertion after chemical induction of LTP has, however, been shown in hippocampal CA1 of *Shank3*$^{e4\text{-}9\ -/-}$ mice (Wang et al. 2011). This suggests a functional dissociation of Shank2 and Shank3 in synaptic maturation - to the extent that the absence of one protein cannot be compensated for by the presence of the other.

4.2.2 Exo-/endocytic cycling of AMPARs

AMPAR trafficking is not implicated in LTP expression only. In fact, membrane trafficking from recycling endosomes seems to be necessary for spine maintenance (Park et al. 2006, Brown et al. 2007) and, paradoxically, constitutive synaptic endocytosis is apprently important for AMPAR accumulation at PSDs (JLu et al. 2007, askolski et al. 2009, Czöndör et al. 2012). Stably positioned sites of clathrin (endocytic zones, EZs; see section 1.4.1) (Blanpied et al. 2002) are localized close to the PSD via a chain of protein-protein interactions involving dynamin-3, Homer, and Shank (Lu et al. 2007). Importantly, the localization of EZs close to the PSD depends on the intact interaction of Shank and Homer (Lu et al. 2007). These synaptic EZs are thought to be responsible for the localized endocytosis of AMPARs, which establishes and maintains an AMPAR pool for local reinsertion into the synaptic membrane. Consequently, synapses without EZs would have difficulties to locally capture and recycle AMPARs back to the synapse. This deficit reportedly results in the subsequent loss of synaptic AMPARs, a decreased A/N ratio, and an increase in the fraction of silent synapses (Lu et al. 2007). Thus, synapses with internal AMPAR cycling mechanisms should be privileged over others in their ability to regulate synaptic strength (Czöndör et al. 2012), and synapses in *Shank2*$^{-/-}$ mice might have

problems in synaptic AMPAR maintenance due to misplaced EZs. It is again puzzling, however, that LTP is intact in *Shank2*$^{-/-}$ mice, as glycine-induced potentiation in cultured neurons is reportedly disturbed in synapses with displaced EZs (Petrini et al. 2009).

4.2.3 Negative control of NMDARs over synapse maturation

Depending on the nature of incoming activity, NMDAR signalling can either increase or decrease synaptic strength by triggering mechanisms that either lead to LTP or LTD (Malenka and Bear 2004). This is also true for the role of NMDARs in synaptic maturation: In addition to the promotion of synapse unsilencing after appropriate synaptic activity (Isaac et al. 1995, Liao et al. 1995, Durand et al. 1996), NMDARs negatively regulate the incorporation of AMPARs into synapses under baseline conditions (Hall et al. 2007, Adesnik et al. 2008, Gray et al. 2011). This negative regulation is thought to affect expression levels of AMPARs and associated proteins as well as their synaptic vs. extrasynaptic localization (Hall and Ghosh 2008). Specifically, overexpression of GluN2B in cultured hippocampal neurons was shown to reduce surface levels of GluR1 both in synaptic as well as extrasynaptic membranes (Kim et al. 2005). This effect was observed in older but not younger cultures, underlining the notion that the downstream signalling pathways might be developmentally regulated, and that different rules might be in place for the regulation of glutamate receptor trafficking in immature vs. mature neurons (Yasuda et al. 2003, Groc et al. 2006).

Juvenile *Shank2*$^{-/-}$ mice (P13-P14) display slightly increased NMDAR currents (see Figure 17), and immunoblot quantification of synaptosomal preparations in adolescent *Shank2*$^{-/-}$ mice (P25) revealed an upregulation of GluN1 and GluN2B (Supplementary Figure 7 in Schmeisser et al. 2012). If indeed *Shank2*$^{-/-}$ mice suffer from a - moderate - increase in NMDAR signalling at developmental stages where this is not appropriate, this could contribute to attenuated synaptic maturation. Such a model would also be in accordance with the occurence of normal - even increased - LTP, as the negative NMDAR signalling under baseline conditions could be overcome by strong synaptic activity, leading to the subsequent incorporation of AMPARs into synapses. Such a model could also help to explain the full expression of LTD in *Shank2*$^{-/-}$ mice in a condition of already reduced basal synaptic transmission.

4.2.4 LTP maintenance and synapse stability

The immature synaptic phenotype of *Shank2*$^{-/-}$ mice could also be due to defects in the preservation of synapses and/or synaptic strength. It has been shown that the maintenance of LTP is dependent on long-lasting changes of the actin cytoskeleton (Fukazawa et al. 2003) and integrin dynamics (Babayan et al. 2012), and that GluA1 has a role in the instruction of structural plasticity (Kopec et al. 2007). Shanks are known to interact with proteins involved

in integrin signalling (Lim et al. 2001) and the modulation of the actin cytoskeleton (Du et al. 1998, Boeckers et al. 2001, Park et al. 2003, Qualmann et al. 2004, Wendholt et al. 2006), as well as with the GluA1 subunit (Uchino et al. 2006). It is thus tempting to speculate that mechanisms ensuring the long-term preservation of synaptic strength could be disturbed in *Shank2*$^{-/-}$ mice.

Apart from that, the ubiquitin/proteasome pathway is a critical regulator of synaptic molecular architecture and thus the long-term maintenance of LTD and LTP (Malenka and Bear 2004). However, the activity-dependent regulation of synaptic protein turnover has been shown to depend on the ubiquitination of only a few PSD proteins, among them Shank and GKAP (Ehlers 2003). The author speculates that ubiquitination of these few proteins could lead to the rapid destabilization and degradation of large postsynaptic protein complexes. Thinking along those lines one might imagine that the loss of Shank2 per se could destabilize synapses, possibly causing a higher synapse turnover and the increased occurence of immature synapses.

4.2.5 Alternative interpretations

In the previous sections of this chapter we have presented some ideas as to how the loss of Shank2 could be responsible for attenuated synaptic maturation in the knockout mice. We have assumed that the deficits in synaptic maturation would then cause the reduced excitatory synaptic transmission we observed in fEPSP and mEPSC recordings. Although this interpretation is intuitive, we do not have proof to justify the causality implied here. In fact, it is also possible that the reduced synaptic maturation in adolescent animals is not cause but consequence of a reduced excitatory synaptic transmission. In such a scenario, we would have to assume that excitatory synaptic transmission in *Shank2*$^{-/-}$ mice was decreased for other (so far unknown) reasons. In consequence, the strong synaptic activity needed to induce synaptic maturation via LTP-like mechanisms might be difficult to be evoked in vivo. A single-cell reconstitution of *Shank2* expression (either via viral injections or in utero electroporation) could help to disentangle the effects of Shank2 in single cells versus neuronal networks. It is interesting in this context that a silent synapse phenotype has recently been described in the striatum of mice lacking Sapap3 (Wan et al. 2011), a protein of the GKAP family that directly interacts with Shanks (Boeckers et al. 1999b, Naisbitt et al. 1999, Yao et al. 1999). Reminiscent of our findings, Sapap3$^{-/-}$ animals display reduced excitatory synaptic transmission, a phenotype that could be acutely reversed by viral gene expression (Welch et al. 2007). Wan and colleagues (2011) show that the reduced synaptic transmission in Sapap3$^{-/-}$ mice can be explained by a high fraction of silent synapses in the striatal neuropil. The authours present evidence that

AMPARs are actively removed from the synapse by excessive mGluR5-induced endocytosis. The investigation of mGluR and IP_3 mediated signalling would be interesting in *Shank2*$^{-/-}$ mice as well (Tu et al. 1999, Hwang et al. 2005), but was beyond the scope of this work.

It also has to be kept in mind that the data presented in this thesis is derived from an acute in vitro brain slice preparation. The removal of the brain from the animal‘s body, the cutting procedure and the subsequent slice storage is known to induce alterations on the molecular and structural level of neurons. These alterations are rather variable and depend on numerous parameters of the study design (Kirov et al. 1999, Fiala et al. 2003, Kirov et al. 2004). It is reassuring in this context that our findings on synaptic maturation in wildtype animals match the available electron microscopy data obtained by perfusion fixation (Nusser et al. 1998, Petralia et al. 1999, Takumi et al. 1999, Racca et al. 2000), a preparation that is thought to represent the in vivo situation (Kirov et al. 1999). Whether the phenotype of the *Shank2*$^{-/-}$ mice, however, is caused by disturbed processes that have occured in vivo as compared to in vitro, cannot be resolved here. However, it is obvious from our data that Shank2 mice do not behave like wildtype animals when it comes to the maturation and/or maintenance of synaptic contacts.

4.3 Conclusion

The results we obtained in the *Shank2*$^{-/-}$ mouse are in accordance with a general role for Shank proteins as regulators or effectors of synapse development and maturation (Sheng and Kim 2000, Sala et al. 2001, Kreienkamp 2008, Grabrucker et al 2011). This also applies to the observations made by the research group of Tobias Böckers (Schmeisser et al. 2012): In mice aged eight weeks, they found spine numbers in Shank2$^{-/-}$ mice to be reduced. PSD length or thickness was not significantly altered. Taken together, these results fit into the broad spectrum of phenotypes that have been reported for other knockout models of this protein family; most of them have reportedly smaller and fewer spines as well as reduced synaptic transmission (see Table 4 of the introduction). Our findings, however, strongly contradict a parallel study carried out in an independently generated *Shank2*$^{-/-}$ mouse line (Won et al. 2012). In the respective study, *Shank2*$^{-/-}$ mice show normal hippocampal AMPAR mediated synaptic transmission, an increased A/N ratio, and strong defects in NMDAR dependent LTP and LTD. On a genomic level, the *Shank2*$^{-/-}$ line of Won et al. (2012) is slightly different from the one we used (Schmeisser et al. 2012). On the protein level, however, both strains are null mutants, leaving little room

for explaining the discrepancies between study outcomes with different knockout strategies. Methodological differences might explain some of the differences observed, and an exchange of mouse lines is hoped to help resolve this issue.

The current view of Shank function in synapse development implies a division of labour between Shank2 and Shank3 on the one hand and Shank1 on the other. Shank2 has been described as a protein that very early localizes to sites of synapse formation, preceding PSD-95 and GluN1 (Boeckers et al. 1999a). It was hence suggested that Shank2 could be involved in the initial steps of PSD assembly, possibly in alliance with Shank3, whereas Shank1 would have a role in mature synapses (Boeckers et al. 2005, Grabrucker et al. 2011). It has been shown that overexpression of Shank1 increases the fraction of mushroom spines, but not the spine number in total (Sala et al. 2001), leading the authors to suggest that spines may need to mature and grow to a certain size before they can be stabilized by Shank1. This hypothesis derives further credit from the fact that Shank1$^{-/-}$ mice show deficits in basal synaptic transmission along with intact long-term plasticity (Hung et al. 2008). Our discovery of a role for Shank2 in synapse maturation may in that light come as a surprise, as it implies a role for Shank2 in later stages of synapse development too. It is interesting to note that this function of Shank2 can apparently not be (fully) compensated by Shank3 or Shank1. This implication is in agreement with the observation that after acute knockdown of Shank2 in primary hippocampal cell cultures increased levels of GluN1 and Shank3 are detected at synapses (Schmeisser et al. 2012), suggestive of a more immature synaptic signature. Another surprising observation in our study is the lack of synaptic maturation deficits in juvenile *Shank2*$^{-/-}$ mice. This indicates that either Shank2 does not fulfill important functions at nascent synapses, or that the functional redundancy of Shank2 and Shank3 is higher in early synapse formation than it is in the later maturation of synaptic contacts. In conclusion, the present work describes a role for Shank2 in the manifestation of synaptic maturation. Further research will be necessary to elucidate the mechanisms by which Shank2 manifests the maturation state of synaptic contacts.

5 References

Adesnik H, Li G, During MJ, Pleasure SJ, Nicoll RA. 2008. NMDA receptors inhibit synapse unsilencing during brain development. Proceedings of the National Academy of Sciences of the United States of America 105: 5597–602

Adesnik H, Nicoll RA, England PM. 2005. Photoinactivation of native AMPA receptors reveals their real-time trafficking. Neuron 48: 977–85

Ahmari SE, Buchanan J, Smith SJ. 2000. Assembly of presynaptic active zones from cytoplasmic transport packets. Nature Neuroscience 3: 445–51

Allison DW, Gelfand VI, Spector I, Craig AM. 1998. Role of actin in anchoring postsynaptic receptors in cultured hippocampal neurons: differential attachment of NMDA versus AMPA receptors. The Journal of Neuroscience 18: 2423–36

Anggono V, Huganir RL. 2012. Regulation of AMPA receptor trafficking and synaptic plasticity. Current Opinion in Neurobiology

Babayan AH, Kramar EA, Barrett RM, Jafari M, Häettig J, Chen LY, Rex CS, Lauterborn JC, Wood MA, Gall CM, Lynch G. 2012. Integrin Dynamics Produce a Delayed Stage of Long-Term Potentiation and Memory Consolidation. The Journal of Neuroscience 32: 12854–12861

Banke TG, Bowie D, Lee H, Huganir RL, Schousboe A, Traynelis SF. 2000. Control of GluR1 AMPA receptor function by cAMP-dependent protein kinase. The Journal of Neuroscience 20: 89–102

Barria A, Malinow R. 2005. NMDA receptor subunit composition controls synaptic plasticity by regulating binding to CaMKII. Neuron 48: 289–301

Barrow SL, Constable JRL, Clark E, El-Sabeawy F, McAllister AK, Washbourne P. 2009. Neuroligin1: a cell adhesion molecule that recruits PSD-95 and NMDA receptors by distinct mechanisms during synaptogenesis. Neural Development 4: 17

Barry MF, Ziff EB. 2002. Receptor trafficking and the plasticity of excitatory synapses. Current Opinion in Neurobiology 12: 279–286

Barth AL, Malenka RC. 2001. NMDAR EPSC kinetics do not regulate the critical period for LTP at thalamo-cortical synapses. Nature Neuroscience 4: 235–6

Bayés A, Lagemaat LN van de, Collins MO, Croning MDR, Whittle IR, Choudhary JS, Grant SGN. 2011. Characterization of the proteome, diseases and evolution of the human postsynaptic density. Nature Neuroscience 14: 19–21

Berkel S, Marshall CR, Weiss B, Howe J, Roeth R, Moog U, Endris V, Roberts W, Szatmari P, Pinto D, Bonin M, Riess A, Engels H, Sprengel R, Scherer SW, Rappold GA. 2010. Mutations in the SHANK2 synaptic scaffolding gene in autism spectrum disorder and mental retardation. Nature Genetics 42: 489–91

Blanpied TA, Scott DB, Ehlers MD. 2002. Dynamics and regulation of clathrin coats at specialized endocytic zones of dendrites and spines. Neuron 36: 435–49

Bockmann J, Kreutz MR, Gundelfinger ED, Boeckers TM. 2002. ProSAP/Shank postsynaptic density proteins interact with insulin receptor tyrosine kinase substrate IRSp53. The Journal of Neurochemistry 83: 1013–7

Boeckers TM. 2006. The postsynaptic density. Cell and Tissue Research 326: 409–22

Boeckers TM, Bockmann J, Kreutz MR, Gundelfinger ED. 2002. ProSAP/Shank proteins - a family of higher order organizing molecules of the postsynaptic density with an emerging role in human neurological disease. The Journal of Neurochemistry 81: 903–10

Boeckers TM, Kreutz MR, Winter C, Zuschratter W, Smalla K-HH, Sanmarti-Vila L, Wex H, Langnaese K, Bockmann J, Garner CC, Gundelfinger ED. 1999. a. Proline-Rich Synapse-Associated Protein-1/Cortactin Binding Protein 1 (ProSAP1/CortBP1) Is a PDZ-Domain Protein Highly Enriched in the Postsynaptic Density. The Journal of Neuroscience 19: 6506–6518

Boeckers TM, Liedtke T, Spilker C, Dresbach T, Bockmann J, Kreutz MR, Gundelfinger ED. 2005. C-terminal synaptic targeting elements for postsynaptic density proteins ProSAP1/Shank2 and ProSAP2/Shank3. The Journal of Neurochemistry 92: 519–24

Boeckers TM, Mameza MG, Kreutz MR, Bockmann J, Weise C, Buck F, Richter D, Gundelfinger ED, Kreienkamp HJ. 2001. Synaptic scaffolding proteins in rat brain. Ankyrin repeats of the multidomain Shank protein family interact with the cytoskeletal protein alpha-fodrin. The Journal of Biological Chemistry 276: 40104–12

Boeckers TM, Segger-Junius M, Iglauer P, Bockmann J, Gundelfinger ED, Kreutz MR, Richter D, Kindler S, Kreienkamp H-J. 2004. Differential expression and dendritic transcript localization of Shank family members: identification of a dendritic targeting element in the 3' untranslated region of Shank1 mRNA. Molecular and Cellular Neurosciences 26: 182–90

Boeckers TM, Winter C, Smalla KH, Kreutz MR, Bockmann J, Seidenbecher C, Garner CC, Gundelfinger ED. 1999. b. Proline-rich synapse-associated proteins ProSAP1 and ProSAP2 interact with synaptic proteins of the SAPAP/GKAP family. Biochemical and Biophysical Research Communications 264: 247–52

Bolshakov VY, Siegelbaum SA. 1995. Regulation of hippocampal transmitter release during development and long-term potentiation. Science 269: 1730–4

Borgdorff AJ, Choquet D. 2002. Regulation of AMPA receptor lateral movements. Nature 417: 649–53

Bozdagi O, Sakurai T, Papapetrou D, Wang X, Dickstein DL, Takahashi N, Kajiwara Y, Yang M, Katz AM, Scattoni ML, Harris MJ, Saxena R, Silverman JL, Crawley JN, Zhou Q, Hof PR, Buxbaum JD. 2010. Haploinsufficiency of the autism-associated Shank3 gene leads to deficits in synaptic function, social interaction, and social communication. Molecular Autism 1: 15

Bresler T, Shapira M, Boeckers TM, Dresbach T, Futter M, Garner CC, Rosenblum K, Gundelfinger ED, Ziv NE. 2004. Postsynaptic density assembly is fundamentally different from presynaptic active zone assembly. The Journal of Neuroscience 24: 1507–20

Brown TC, Correia SS, Petrok CN, Esteban JA. 2007. Functional compartmentalization of endosomal trafficking for the synaptic delivery of AMPA receptors during long-term potentiation. The Journal of Neuroscience 27: 13311–5

Calabrese B, Wilson MS, Halpain S. 2006. Development and regulation of dendritic spine synapses. Physiology 21: 38–47

Carmignoto G, Vicini S. 1992. Activity-dependent decrease in NMDA receptor responses during development of the visual cortex. Science 258: 1007–1011

Cingolani LA, Goda Y. 2008. Actin in action: the interplay between the actin cytoskeleton and synaptic efficacy. Nature Reviews Neuroscience 9: 344–56

Cooney JR, Hurlburt JL, Selig DK, Harris KM, Fiala JC. 2002. Endosomal compartments serve multiple hippocampal dendritic spines from a widespread rather than a local store of recycling membrane. The Journal of Neuroscience 22: 2215–24

Craven SE, Bredt DS. 1998. PDZ Proteins Organize Synaptic Signaling Pathways. Cell 93: 495–498

Cruz-Martín A, Crespo M, Portera-Cailliau C. 2010. Delayed stabilization of dendritic spines in fragile X mice. The Journal of Neurosciencence 30: 7793–803

Cull-Candy SG, Kelly L, Farrant M. 2006. Regulation of Ca^{2+}-permeable AMPA receptors: synaptic plasticity and beyond. Current Opinion in Neurobiology 16: 288–97

Czöndör K, Mondin M, Garcia M, Heine M, Frischknecht R, Choquet D, Sibarita J-B, Thoumine OR. 2012. Unified quantitative model of AMPA receptor trafficking at synapses. Proceedings of the National Academy of Sciences of the United States of America

Du Y, Weed SA, Xiong WC, Marshall TD, Parsons JT. 1998. Identification of a novel cortactin SH3 domain-binding protein and its localization to growth cones of cultured neurons. Molecular and Cellular Biology 18: 5838–51

Durand CM, Betancur C, Boeckers TM, Bockmann J, Chaste P, Fauchereau F, Nygren G, Rastam M, Gillberg IC, Anckarsäter H, Sponheim E, Goubran-Botros H, Delorme R, Chabane N, Mouren-Simeoni M-C, Mas P de, Bieth E, Rogé B, Héron D, Burglen L, Gillberg C, Leboyer M, Bourgeron T. 2007. Mutations in the gene encoding the synaptic scaffolding protein SHANK3 are associated with autism spectrum disorders. Nature Genetics 39: 25–7

Durand GM, Kovalchuk Y, Konnerth A. 1996. Long-term potentiation and functional synapse induction in developing hippocampus. Nature 381: 71–75

Durand CM, Perroy J, Loll F, Perrais D, Fagni L, Bourgeron T, Montcouquiol M, Sans N. 2011. SHANK3 mutations identified in autism lead to modification of dendritic spine morphology via an actin-dependent mechanism. Molecular Psychiatry: 1–14

Ehlers MD. 2000. Reinsertion or degradation of AMPA receptors determined by activity-dependent endocytic sorting. Neuron 28: 511–25

Ehlers MD. 2003. Activity level controls postsynaptic composition and signaling via the ubiquitin-proteasome system. Nature Neuroscience 6: 231–42

Feng W, Zhang M. 2009. Organization and dynamics of PDZ-domain-related supramodules in the postsynaptic density. Nature Reviews Neuroscience 10: 87–99

Fernandez-Monreal M, Brown TC, Royo M, Esteban JA. 2012. The Balance between Receptor Recycling and Trafficking toward Lysosomes Determines Synaptic Strength during Long-Term Depression. The Journal of Neuroscience 32: 13200–13205

Fischer M, Kaech S, Knutti D, Matus A. 1998. Rapid Actin-Based Plasticity in Dendritic Spines. Neuron 20: 847–854

Fischer M, Kaech S, Wagner U, Brinkhaus H, Matus A. 2000. Glutamate receptors regulate actin-based plasticity in dendritic spines. Nature Neuroscience 3: 887–94

Flint AC, Maisch US, Weishaupt JH, Kriegstein AR, Monyer H. 1997. NR2A Subunit Expression Shortens NMDA Receptor Synaptic Currents in Developing Neocortex. The Journal of Neuroscience 17: 2469–2476

Foster KA, McLaughlin N, Edbauer D, Phillips M, Bolton A, Constantine-Paton M, Sheng M. 2010. Distinct roles of NR2A and NR2B cytoplasmic tails in long-term potentiation. The Journal of Neuroscience 30: 2676–85

Franks KM, Isaacson JS. 2005. Synapse-specific downregulation of NMDA receptors by early experience: a critical period for plasticity of sensory input to olfactory cortex. Neuron 47: 101–14

Frost N, Kerr J, Lu H, Blanpied T. 2010. A network of networks: cytoskeletal control of compartmentalized function within dendritic spines. Current Opinion in Neurobiology 20: 578–587

Fukazawa Y, Saitoh Y, Ozawa F, Ohta Y, Mizuno K, Inokuchi K. 2003. Hippocampal LTP is accompanied by enhanced F-actin content within the dendritic spine that is essential for late LTP maintenance in vivo. Neuron 38: 447–60

Garcia-Lopez P, Garcia-Marín V, Freire M. 2010. The histological slides and drawings of cajal. Frontiers in Neuroanatomy 4: 9

Gerrow K, Romorini S, Nabi SM, Colicos M a, Sala C, El-Husseini AE. 2006. A preformed complex of postsynaptic proteins is involved in excitatory synapse development. Neuron 49: 547–62

Gladding CM, Collett VJ, Jia Z, Bashir ZI, Collingridge GL, Molnár E. 2009. Tyrosine dephosphorylation regulates AMPAR internalisation in mGluR-LTD. Molecular and Cellular Neurosciences 40: 267–79

Gong Y, Lippa CF, Zhu J, Lin Q, Rosso AL. 2009. Disruption of glutamate receptors at Shank-postsynaptic platform in Alzheimer's disease. Brain Research 1292: 191–8

Grabrucker AM, Knight MJ, Proepper C, Bockmann J, Joubert M, Rowan M, Nienhaus GU, Garner CC, Bowie JU, Kreutz MR, Gundelfinger ED, Boeckers TM. 2011. Concerted action of zinc and ProSAP/Shank in synaptogenesis and synapse maturation. The EMBO Journal 30: 569–81

Gray EG. 1959. Electron Microscopy of Synaptic Contacts on Dendrite Spines of the Cerebral Cortex. Nature 183: 1592–1593

Gray JA, Shi Y, Usui H, During MJ, Sakimura K, Nicoll RA. 2011. Distinct Modes of AMPA Receptor Suppression at Developing Synapses by GluN2A and GluN2B: Single-Cell NMDA Receptor Subunit Deletion In Vivo. Neuron 71: 1085–1101

Greger IH, Esteban J a. 2007. AMPA receptor biogenesis and trafficking. Current Opinion in Neurobiology 17: 289–97

Greger IH, Khatri L, Kong X, Ziff E. 2003. AMPA receptor tetramerization is mediated by Q/R editing. Neuron 40: 763–774

Groc L, Bard L, Choquet D. 2009. Surface trafficking of N-methyl-D-aspartate receptors: physiological and pathological perspectives. Neuroscience 158: 4–18

Groc L, Gustafsson B, Hanse E. 2006. AMPA signalling in nascent glutamatergic synapses: there and not there! Trends in Neurosciences 29: 132–9

Grutzendler J, Kasthuri N, Gan W-B. 2002. Long-term dendritic spine stability in the adult cortex. Nature 420: 812–6

Hall BJ, Ghosh A. 2008. Regulation of AMPA receptor recruitment at developing synapses. Trends in Neurosciences 31: 82–9

Hall BJ, Ripley B, Ghosh A. 2007. NR2B signaling regulates the development of synaptic AMPA receptor current. The Journal of Neuroscience 27: 13446–56

Hardingham GE, Bading H. 2010. Synaptic versus extrasynaptic NMDA receptor signalling: implications for neurodegenerative disorders. Nature Reviews Neuroscience 11: 682–96

Harris KM, Jensen FE, Tsao B. 1992. Three-dimensional structure of dendritic spines and synapses in rat hippocampus (CA1) at postnatal day 15 and adult ages: implications for the maturation of synaptic physiology and long-term potentiation. The Journal of Neuroscience 12: 2685–705

Hayashi Y, Shi SH, Esteban JA, Piccini A, Poncer JC, Malinow R, S-H S, JA E, A P, J-C P. 2000. Driving AMPA Receptors into Synapses by LTP and CaMKII: Requirement for GluR1 and PDZ Domain Interaction. Science 287: 2262–2267

Hayashi MK, Tang C, Verpelli C, Narayanan R, Stearns MH, Xu R-M, Li H, Sala C, Hayashi Y. 2009. The postsynaptic density proteins Homer and Shank form a polymeric network structure. Cell 137: 159–71

Hering H, Sheng M. 2001. Dendritic spines: structure, dynamics and regulation. Nature Reviews Neuroscience 2: 880–8

Hestrin S. 1992. Developmental regulation of NMDA receptor-mediated synaptic currents at a central synapse. Nature 357: 686–9

Heynen AJ, Quinlan EM, Bae DC, Bear MF. 2000. Bidirectional, Activity-Dependent Regulation of Glutamate Receptors in the Adult Hippocampus In Vivo. Neuron 28: 527–536

Hollmann M, Hartley M, Heinemann S. 1991. Ca^{2+} permeability of KA-AMPA-gated glutamate receptor channels depends on subunit composition. Science 252: 851–3

Hollmann M, Heinemann SF. 1994. Cloned glutamate receptors. Annual Review of Neuroscience: 31–108

Hotulainen P, Hoogenraad CC. 2010. Actin in dendritic spines: connecting dynamics to function. The Journal of Cell Biology 189: 619–29

Hsia A, Malenka RC, Nicoll RA. 1998. Development of excitatory circuitry in the hippocampus. Journal of Neurophysiology: 2013–2024

Hua JY, Smith SJ. 2004. Neural activity and the dynamics of central nervous system development. Nature Neuroscience 7: 327–32

Hung AY, Futai K, Sala C, Valtschanoff JG, Ryu J, Woodworth M a, Kidd FL, Sung CC, Miyakawa T, Bear MF, Weinberg RJ, Sheng M. 2008. Smaller dendritic spines, weaker synaptic transmission, but enhanced spatial learning in mice lacking Shank1. The Journal of Neuroscience 28: 1697–708

Hwang J-I, Kim HS, Lee JR, Kim E, Ryu SH, Suh P-G. 2005. The interaction of phospholipase C-beta3 with Shank2 regulates mGluR-mediated calcium signal. The Journal of Biological Chemistry 280: 12467–73

Im YJ, Lee JH, Park SH, Park SJ, Rho S-H, Kang GB, Kim E, Eom SH. 2003. Crystal structure of the Shank PDZ-ligand complex reveals a class I PDZ interaction and a novel PDZ-PDZ dimerization. The Journal of Biological Chemistry 278: 48099–104

Isaac JTR, Lüthi A, Palmer MJ, Anderson WW, Benke TA, Collingridge GL. 1997. Silent synapses during development of thalamocortical inputs. Neuron 18: 269–80

Isaac JTR, Nicoll RA, Malenka RC. 1995. Evidence for silent synapses: implications for the expression of LTP. Neuron 15: 427–34

Ishii T, Moriyoshi K, Sugihara H, Sakurada K, Kadotani H, Yokoi M, Akazawa C, Shigemoto R, Mizuno N, Masu M. 1993. Molecular characterization of the family of the N-methyl-D-aspartate receptor subunits. The Journal of Biological Chemistry 268: 2836–2843

Jaskolski F, Mayo-Martin B, Jane D, Henley JM. 2009. Dynamin-dependent membrane drift recruits AMPA receptors to dendritic spines. The Journal of Biological Chemistry 284: 12491–503

Jia Z, Agopyan N, Miu P, Xiong Z, Henderson J, Gerlai R, Taverna FA, Velumian A, MacDonald J, Carlen P, Abramow-Newerly W, Roder J. 1996. Enhanced LTP in mice deficient in the AMPA receptor GluR2. Neuron 17: 945–56

Kay L, Humphreys L, Eickholt BJ, Burrone J. 2011. Neuronal activity drives matching of pre- and postsynaptic function during synapse maturation. Nature Neuroscience 14: 688–90

Kennedy MB. 2000. Signal-Processing Machines at the Postsynaptic Density. Science 290: 750–754

Kennedy MJ, Ehlers MD. 2011. Mechanisms and function of dendritic exocytosis. Neuron 69: 856–75

Kim S-M, Choi KY, Cho IH, Rhy JH, Kim SH, Park C-S, Kim E, Song WK. 2009. Regulation of dendritic spine morphology by SPIN90, a novel Shank binding partner. The Journal of Neurochemistry 109: 1106–17

Kim MJ, Dunah AW, Wang YT, Sheng M. 2005. Differential roles of NR2A- and NR2B-containing NMDA receptors in Ras-ERK signaling and AMPA receptor trafficking. Neuron 46: 745–60

Kim CH, Lisman JE. 1999. A role of actin filament in synaptic transmission and long-term potentiation. The Journal of Neuroscience 19: 4314–24

Kim E, Sheng M. 2004. PDZ domain proteins of synapses. Nature Reviews Neuroscience 5: 771–81

Kopec CD, Real E, Kessels HW, Malinow R. 2007. GluR1 links structural and functional plasticity at excitatory synapses. The Journal of Neuroscience 27: 13706–18

Kreienkamp HJ. 2008. Scaffolding proteins at the postsynaptic density: shank as the architectural framework. Handbook of Experimental Pharmacology: 365–80

Kreienkamp HJ, Zitzer H, Gundelfinger ED, Richter D, Boeckers TM. 2000. The calcium-independent receptor for alpha-latrotoxin from human and rodent brains interacts with members of the ProSAP/SSTRIP/Shank family of multidomain proteins. The Journal of Biological Chemistry 275: 32387–90

Krucker T, Siggins GR, Halpain S. 2000. Dynamic actin filaments are required for stable long-term potentiation (LTP) in area CA1 of the hippocampus. Proceedings of the National Academy of Sciences of the United States of America 97: 6856–61

Kullmann DM. 1994. Amplitude fluctuations of dual-component EPSCs in hippocampal pyramidal cells: implications for long-term potentiation. Neuron 12: 1111–20

Kuriu T, Inoue A, Bito H, Sobue K, Okabe S. 2006. Differential control of postsynaptic density scaffolds via actin-dependent and -independent mechanisms. The Journal of Neuroscience 26: 7693–706

Lee SH, Liu L, Wang YT, Sheng M. 2002. Clathrin adaptor AP2 and NSF interact with overlapping sites of GluR2 and play distinct roles in AMPA receptor trafficking and hippocampal LTD. Neuron 36: 661–74

Lendvai B, Stern EA, Chen B, Svoboda K. 2000. Experience-dependent plasticity of dendritic spines in the developing rat barrel cortex in vivo. Nature 404: 876–81

Lester RA, Clements JD, Westbrook GL, Jahr CE. 1990. Channel kinetics determine the time course of NMDA receptor-mediated synaptic currents. Nature 346: 565–7

Liao D, Hessler N, Malinow R. 1995. Activation of postsynaptically silent synapses during pairing-induced LTP in CA1 region of hippocampal slice. Nature 375: 400–4

Liao D, Zhang X, O'Brien RJ, Ehlers MD, Huganir RL. 1999. Regulation of morphological postsynaptic silent synapses in developing hippocampal neurons. Nature Neuroscience 2: 37–43

Lichtman JW, Colman H. 2000. Synapse Elimination and Indelible Memory. Neuron 25: 269–278

Lim S, Naisbitt S, Yoon J, Hwang J-I, Suh P-G, And MS, Kim E. 1999. Characterization of the Shank Family of Synaptic Proteins. Multiple Genes, Alternative Splicing, and Differential Expression in Brain and Development. The Journal of Biological Chemistry 274: 29510–29518

Lim S, Sala C, Yoon J, Park S, Kuroda S, Sheng M, Kim E. 2001. Sharpin, a novel postsynaptic density protein that directly interacts with the shank family of proteins. Molecular and Cellular Neurosciences 17: 385–97

Lin JW, Ju W, Foster K, Lee SH, Ahmadian G, Wyszynski M, Wang YT, Sheng M. 2000. Distinct molecular mechanisms and divergent endocytotic pathways of AMPA receptor internalization. Nature Neuroscience 3: 1282–1290

Lin D-T, Makino Y, Sharma K, Hayashi T, Neve R, Takamiya K, Huganir RL. 2009. Regulation of AMPA receptor extrasynaptic insertion by 4.1N, phosphorylation and palmitoylation. Nature Neuroscience 12: 879–87

Lomeli H, Mosbacher J, Melcher T, Höger T, Geiger JR, Kuner T, Monyer H, Higuchi M, Bach A, Seeburg PH. 1994. Control of kinetic properties of AMPA receptor channels by nuclear RNA editing. Science 266: 1709–13

Lu J, Helton TD, Blanpied TA, Rácz B, Newpher TM, Weinberg RJ, Ehlers MD. 2007. Postsynaptic Positioning of Endocytic Zones and AMPA Receptor Cycling by Physical Coupling of Dynamin-3 to Homer. Neuron 55: e7–13

Lu W, Shi Y, Jackson AC, Bjorgan K, During MJ, Sprengel R, Seeburg PH, Nicoll R a. 2009. Subunit composition of synaptic AMPA receptors revealed by a single-cell genetic approach. Neuron 62: 254–68

Lüscher C, Xia H, Beattie EC, Carroll RC, Zastrow M von, Malenka RC, Nicoll RA. 1999. Role of AMPA receptor cycling in synaptic transmission and plasticity. Neuron 24: 649–58

MacDermott A, Mayer ML, Westbrook GL, Smith SJ, Barker JL. 1986. NMDA-receptor activation increases cytoplasmic calcium concentration in cultured spinal cord neurones. Nature 321: 519–22

Makino H, Malinow R. 2009. AMPA receptor incorporation into synapses during LTP: the role of lateral movement and exocytosis. Neuron 64: 381–90

Malenka RC, Bear MF. 2004. LTP and LTD: an embarrassment of riches. Neuron 44: 5–21

Malinow R, Malenka RC. 2002. AMPA receptor trafficking and synaptic plasticity. Annual Review of Neuroscience 25: 103–26

Mano I, Teichberg VI. 1998. A tetrameric subunit stoichiometry for a glutamate receptor-channel complex. Neuroreport 9: 327–31

Mansour M, Nagarajan N, Nehring RB, Clements JD, Rosenmund C. 2001. Heteromeric AMPA Receptors Assemble with a Preferred Subunit Stoichiometry and Spatial Arrangement. Neuron 32: 841–853

Matsuzaki M, Honkura N, Ellis-Davies GCR, Kasai H. 2004. Structural basis of long-term potentiation in single dendritic spines. Nature 429: 761–6

McAllister AK. 2007. Dynamic aspects of CNS synapse formation. Annual Review Neuroscience: 425–450

McWilliams RR, Gidey E, Fouassier L, Weed S a, Doctor RB. 2004. Characterization of an ankyrin repeat-containing Shank2 isoform (Shank2E) in liver epithelial cells. The Biochemical Journal 380: 181–91

Megías M, Emri Z, Freund TF, Gulyás AI, Gulyas A. 2001. Total Number and Distribution of Inhibitory and Excitatory Synapses on Hippocampal CA1 Pyramidal Cells. Neuroscience 102: 527–540

Monyer H, Burnashev N, Laurie DJ, Sakmann B, Seeburg PH. 1994. Developmental and regional expression in the rat brain and functional properties of four NMDA receptors. Neuron 12: 529–540

Monyer H, Sprengel R, Schoepfer R, Herb A, Higuchi M, Lomeli H, Burnashev N, Sakmann B, Seeburg PH. 1992. Heteromeric NMDA receptors: molecular and functional distinction of subtypes. Science 256: 1217–1221

Murakoshi H, Yasuda R. 2012. Postsynaptic signaling during plasticity of dendritic spines. Trends in Neurosciences 35: 135–43

Naisbitt S, Kim E, Tu JC, Xiao B, Sala C, Valtschanoff JG, Weinberg RJ, Worley PF, Sheng M. 1999. Shank, a novel family of postsynaptic density proteins that binds to the NMDA receptor/PSD-95/GKAP complex and cortactin. Neuron 23: 569–82

Nakagawa T. 2010. The biochemistry, ultrastructure, and subunit assembly mechanism of AMPA receptors. Molecular Neurobiology 42: 161–84

Newpher TM, Ehlers MD. 2009. Spine microdomains for postsynaptic signaling and plasticity. Trends in Cell Biology 19: 218–27

Nimchinsky EA, Sabatini BL, Svoboda K. 2002. Structure and function of dendritic spines. Annual Review of Physiology 64: 313–53

Noguchi J, Matsuzaki M, Ellis-Davies GCR, Kasai H. 2005. Spine-neck geometry determines NMDA receptor-dependent Ca^{2+} signaling in dendrites. Neuron 46: 609–22

Nowak L, Bregestovski P, Ascher P, Herbet A, Prochiantz A. 1984. Magnesium gates glutamate-activated channels in mouse central neurones. Nature 307: 462–5

Nusser Z, Lujan R, Laube G, Roberts JD, Molnar E, Somogyi P. 1998. Cell type and pathway dependence of synaptic AMPA receptor number and variability in the hippocampus. Neuron 21: 545–59

Okamoto PM, Gamby C, Wells D, Fallon J, Vallee RB. 2001. Dynamin isoform-specific interaction with the shank/ProSAP scaffolding proteins of the postsynaptic density and actin cytoskeleton. The Journal of Biological Chemistry 276: 48458–65

Papouin T, Ladépêche L, Ruel J, Sacchi S, Labasque M, Hanini M, Groc L, Pollegioni L, Mothet J-P, Oliet SHR. 2012. Synaptic and Extrasynaptic NMDA Receptors Are Gated by Different Endogenous Coagonists. Cell 150: 633–646

Park E, Na M, Choi J, Kim S, Lee J-R, Yoon J, Park D, Sheng M, Kim E. 2003. The Shank family of postsynaptic density proteins interacts with and promotes synaptic accumulation of the beta PIX guanine nucleotide exchange factor for Rac1 and Cdc42. The Journal of Biological Chemistry 278: 19220–9

Park M, Salgado JM, Ostroff L, Helton TD, Robinson CG, Harris KM, Ehlers MD. 2006. Plasticity-induced growth of dendritic spines by exocytic trafficking from recycling endosomes. Neuron 52: 817–830

Passafaro M, Nakagawa T, Sala C, Sheng M. 2003. Induction of dendritic spines by an extracellular domain of AMPA receptor subunit GluR2. Nature 424: 677–81

Passafaro M, Piëch V, Sheng M. 2001. Subunit-specific temporal and spatial patterns of AMPA receptor exocytosis in hippocampal neurons. Nature Neuroscience 4: 917–26

Patterson MA, Szatmari EM, Yasuda R. 2010. AMPA receptors are exocytosed in stimulated spines and adjacent dendrites in a Ras-ERK-dependent manner during long-term potentiation. Proceedings of the National Academy of Sciences of the United States of America 107: 15951–6

Petralia RS, Esteban JA, Wang YX, Partridge JG, Zhao HM, Wenthold RJ, Malinow R. 1999. Selective acquisition of AMPA receptors over postnatal development suggests a molecular basis for silent synapses. Nature Neuroscience 2: 31–6

Petralia RS, Sans N, Wang Y-X, Wenthold RJ. 2005. Ontogeny of postsynaptic density proteins at glutamatergic synapses. Molecular and Cellular Neurosciences 29: 436–52

Petrini EM, Lu J, Cognet L, Lounis B, Ehlers MD, Choquet D. 2009. Endocytic trafficking and recycling maintain a pool of mobile surface AMPA receptors required for synaptic potentiation. Neuron 63: 92–105

Peça J, Feliciano C, Ting JT, Wang W, Wells MF, Venkatraman TN, Lascola CD, Fu Z, Feng G. 2011. Shank3 mutant mice display autistic-like behaviours and striatal dysfunction. Nature 472: 437–42

Pham E, Crews L, Ubhi K, Hansen L, Adame A, Cartier A, Salmon D, Galasko D, Michael S, Savas JN, Yates JR, Glabe C, Masliah E. 2010. Progressive accumulation of amyloid-beta oligomers in Alzheimer's disease and in amyloid precursor protein transgenic mice is accompanied by selective alterations in synaptic scaffold proteins. The FEBS Journal 277: 3051–67

Puchalski RB, Louis JC, Brose N, Traynelis SF, Egebjerg J, Kukekov V, Wenthold RJ, Rogers SW, Lin F, Moran T. 1994. Selective RNA editing and subunit assembly of native glutamate receptors. Neuron 13: 131–47

Qualmann B, Boeckers TM, Jeromin M, Gundelfinger ED, Kessels MM. 2004. Linkage of the actin cytoskeleton to the postsynaptic density via direct interactions of Abp1 with the ProSAP/Shank family. The Journal of Neuroscience 24: 2481–95

Racca C, Stephenson FA, Streit P, Roberts JD, Somogyi P. 2000. NMDA receptor content of synapses in stratum radiatum of the hippocampal CA1 area. The Journal of Neuroscience 20: 2512–22

Rao A, Kim E, Sheng M, Craig AM. 1998. Heterogeneity in the molecular composition of excitatory postsynaptic sites during development of hippocampal neurons in culture. The Journal of Neuroscience 18: 1217–29

Rauner C, Köhr G. 2011. Triheteromeric NR1/NR2A/NR2B receptors constitute the major N-methyl-D-aspartate receptor population in adult hippocampal synapses. The Journal of Biological Chemistry 286: 7558–66

Redecker P, Gundelfinger ED, Boeckers TM. 2001. The Cortactin-binding Postsynaptic Density Protein ProSAP1 in Non-neuronal Cells. Journal of Histochemistry & Cytochemistry 49: 639–648

Robinson JH, Deadwyler SA. 1981. Kainic acid produces depolarization of CA3 pyramidal cells in the vitro hippocampal slice. Brain Research 221: 117–27

Roselli F, Hutzler P, Wegerich Y, Livrea P, Almeida OFX. 2009. Disassembly of shank and homer synaptic clusters is driven by soluble beta-amyloid(1-40) through divergent NMDAR-dependent signalling pathways. PloS ONE 4: e6011

Rosenmund C, Stern-Bach Y, Stevens CF. 1998. The Tetrameric Structure of a Glutamate Receptor Channel. Science 280: 1596–1599

Roussignol G, Ango F, Romorini S, Tu JC, Sala C, Worley PF, Bockaert J, Fagni L. 2005. Shank expression is sufficient to induce functional dendritic spine synapses in aspiny neurons. The Journal of Neuroscience 25: 3560–70

Rozov A, Sprengel R, Seeburg PH. 2012. GluA2-lacking AMPA receptors in hippocampal CA1 cell synapses: evidence from gene-targeted mice. Frontiers in molecular neuroscience 5: 22

Rumpel S, Hatt H, Gottmann K. 1998. Silent Synapses in the Developing Rat Visual Cortex: Evidence for Postsynaptic Expression of Synaptic Plasticity. The Journal of Neuroscience 18: 8863–8874

Rácz B, Blanpied TA, Ehlers MD, Weinberg RJ. 2004. Lateral organization of endocytic machinery in dendritic spines. Nature Neuroscience 7: 917–8

Sabo SL, Gomes RA, McAllister AK. 2006. Formation of presynaptic terminals at predefined sites along axons. The Journal of Neuroscience 26: 10813–25

Saglietti L, Dequidt C, Kamieniarz K, Rousset M-C, Valnegri P, Thoumine O, Beretta F, Fagni L, Choquet D, Sala C, Sheng M, Passafaro M. 2007. Extracellular interactions between GluR2 and N-cadherin in spine regulation. Neuron 54: 461–77

Sala C, Piëch V, Wilson NR, Passafaro M, Liu G, Sheng M. 2001. Regulation of Dendritic Spine Morphology and Synaptic Function by Shank and Homer. Neuron 31: 115–130

Sala C, Roussignol G, Meldolesi J, Fagni L. 2005. Key role of the postsynaptic density scaffold proteins Shank and Homer in the functional architecture of Ca^{2+} homeostasis at dendritic spines in hippocampal neurons. The Journal of Neuroscience 25: 4587–92

Sambrook J, Russel DW. 2001. . Molecular Cloning: A Laboratory Manual 3rd Editio. Cold Spring Harbor, New York: Cold Spring Harbor Laboratory Press.

Saneyoshi T, Fortin DA, Soderling TR. 2010. Regulation of spine and synapse formation by activity-dependent intracellular signaling pathways. Current Opinion in Neurobiology 20: 108–15

Sato D, Lionel AC, Leblond CS, Prasad A, Pinto D, Walker S, O'Connor I, Russell C, Drmic IE, Hamdan FF, Michaud JL, Endris V, Roeth R, Delorme R, Huguet G, Leboyer M, Rastam M, Gillberg C, Lathrop M, Stavropoulos DJ, Anagnostou E, Weksberg R, Fombonne E, Zwaigenbaum L, Fernandez BA, Roberts W, Rappold GA, Marshall CR, Bourgeron T, Szatmari P, Scherer SW. 2012. SHANK1 Deletions in Males with Autism Spectrum Disorder. American Journal of Human Genetics 90: 879–87

Schafer DA, Weed SA, Binns D, Karginov A V, Parsons JT, Cooper J a. 2002. Dynamin2 and cortactin regulate actin assembly and filament organization. Current Biology 12: 1852–7

Schikorski T, Stevens CF. 1997. Quantitative ultrastructural analysis of hippocampal excitatory synapses. Journal of Neuroscience 17: 5858–67

Schmeisser M, Ey E, Wegener S, Bockmann J, Stempel AV, Kuebler A, Janssen A-L, Udvardi PT, Shiban E, Spilker C, Balschun D, Skryabin B V., Dieck S tom, Smalla K-H, Montag D, Leblond CS, Faure P, Torquet N, Sourd A-M Le, Toro R, Grabrucker AM, Shoichet SA, Schmitz D, Kreutz MR, Bourgeron T, Gundelfinger ED, Boeckers TM. 2012. Autistic-like behaviours and hyperactivity in mice lacking ProSAP1/Shank2. Nature 486: 256–60

Scholz R, Berberich S, Rathgeber L, Kolleker A, Köhr G, Kornau H-C. 2010. AMPA receptor signaling through BRAG2 and Arf6 critical for long-term synaptic depression. Neuron 66: 768–80

Sdrulla AD, Linden DJ. 2007. Double dissociation between long-term depression and dendritic spine morphology in cerebellar Purkinje cells. Nature Neuroscience 10: 546–8

Sheng M, Cummings J, Roldan LA, Jan YN, Jan LY. 1994. Changing subunit composition of heteromeric NMDA receptors during development of rat cortex. Nature 368: 144–7

Sheng M, Hoogenraad CC. 2007. The postsynaptic architecture of excitatory synapses: a more quantitative view. Annual Review of Biochemistry 76: 823–47

Sheng M, Kim E. 2000. The Shank family of scaffold proteins. Journal of Cell Science 113: 1851–6

Sheng M, Pak D. 2000. Ligand-gated ion channel interactions with cytoskeletal and signaling proteins. Annual Review of Physiology 62: 755–78

Shi S, Hayashi Y, Esteban J, Malinow R. 2001. Subunit-specific rules governing AMPA receptor trafficking to synapses in hippocampal pyramidal neurons. Cell 105: 331–43

Shi S, Hayashi Y, Petralia RS, Zaman SH, Wenthold RJ, Svoboda K, Malinow R. 1999. Rapid spine delivery and redistribution of AMPA receptors after synaptic NMDA receptor activation. Science 284: 1811–6

Shinohara Y. 2011. Quantification of postsynaptic density proteins: Glutamate receptor subunits and scaffolding proteins. Hippocampus 22: 942–53

Singh P, Hockenberry AJ, Tiruvadi VR, Meaney DF. 2011. Computational investigation of the changing patterns of subtype specific NMDA receptor activation during physiological glutamatergic neurotransmission. PLoS Computational Biology 7: e1002106

Soltau M, Richter D, Kreienkamp HJ. 2002. The insulin receptor substrate IRSp53 links postsynaptic shank1 to the small G-protein cdc42. Molecular and Cellular Neuroscience 21: 575–583

Sommer B, Keinänen K, Verdoorn T, Wisden W, Burnashev N, Herb A, Köhler M, Takagi T, Sakmann B, Seeburg PH. 1990. Flip and flop: a cell-specific functional switch in glutamate-operated channels of the CNS. Science 249: 1580–5

Sommer B, Köhler M, Sprengel R, Seeburg PH. 1991. RNA editing in brain controls a determinant of ion flow in glutamate-gated channels. Cell 67: 11–9

Somogyi P, Tamás G, Lujan R, Buhl EH. 1998. Salient features of synaptic organisation in the cerebral cortex. Brain Research Reviews 26: 113–35

Sorra KE, Harris M. 2000. Overview on the structure, composition, function, development, and plasticity of hippocampal dendritic spines. Hippocampus 10: 501–11

Star EN, Kwiatkowski DJ, Murthy VN. 2002. Rapid turnover of actin in dendritic spines and its regulation by activity. Nature Neuroscience 5: 239–46

Swanson GT, Kamboj SK, Cull-Candy SG. 1997. Single-Channel Properties of Recombinant AMPA Receptors Depend on RNA Editing, Splice Variation, and Subunit Composition. The Journal of Neuroscience 17: 58–69

Swulius MT, Kubota Y, Forest A, Waxham MN. 2010. Structure and composition of the postsynaptic density during development. The Journal of Comparative Neurology 518: 4243–60

Takumi Y, Ramírez-León V, Laake P, Rinvik E, Ottersen OP. 1999. Different modes of expression of AMPA and NMDA receptors in hippocampal synapses. Nature Neuroscience 2: 618–24

Tobaben S, Südhof TC, Stahl B. 2000. The G protein-coupled receptor CL1 interacts directly with proteins of the Shank family. The Journal of Biological Chemistry 275: 36204–10

Tomita S. 2010. Regulation of ionotropic glutamate receptors by their auxiliary subunits. Physiology 25: 41–9

Trachtenberg JT, Chen BE, Knott GW, Feng G, Sanes JR, Welker E, Svoboda K. 2002. Long-term in vivo imaging of experience-dependent synaptic plasticity in adult cortex. Nature 420: 788–94

Tu JC, Xiao B, Naisbitt S, Yuan JP, Petralia RS, Brakeman PR, Doan A, Aakalu VK, Lanahan AA, Sheng M, Worley PF. 1999. Coupling of mGluR/Homer and PSD-95 complexes by the Shank family of postsynaptic density proteins. Neuron 23: 583–92

Uchino S, Wada H, Honda S, Nakamura Y, Ondo Y, Uchiyama T, Tsutsumi M, Suzuki E, Hirasawa T, Kohsaka S. 2006. Direct interaction of post-synaptic density-95/Dlg/ZO-1 domain-containing synaptic molecule Shank3 with GluR1 alpha-amino-3-hydroxy-5-methyl-4-isoxazole propionic acid receptor. The Journal of Neurochemistry 97: 1203–14

Valtschanoff JG, Weinberg RJ. 2001. Laminar organization of the NMDA receptor complex within the postsynaptic density. The Journal of Neuroscience 21: 1211–7

Verdoorn TA, Burnashev N, Monyer H, Seeburg PH, Sakmann B. 1991. Structural determinants of ion flow through recombinant glutamate receptor channels. Science 26: 1715–8

Verpelli C, Dvoretskova E, Vicidomini C, Rossi F, Chiappalone M, Schoen M, Stefano B Di, Mantegazza R, Broccoli V, Boeckers TM, Dityatev A, Sala C. 2011. Importance of Shank3 protein in regulating metabotropic glutamate receptor 5 (mGluR5) expression and signaling at synapses. The Journal of Biological Chemistry 286: 34839–50

Vicini S, Wang JF, Li JH, Zhu WJ, Wang YH, Luo JH, Wolfe BB, Grayson DR. 1998. Functional and Pharmacological Differences Between Recombinant N-Methyl-D-Aspartate Receptors. The Journal of Neurophysiology 79: 555–566

Waites CL, Craig AM, Garner CC. 2005. Mechanisms of vertebrate synaptogenesis. Annual Review Neuroscience 28: 251–74

Wan Y, Feng G, Calakos N. 2011. Sapap3 Deletion Causes mGluR5-Dependent Silencing of AMPAR Synapses. The Journal of Neuroscience 31: 16685–91

Wang X, McCoy PA, Rodriguiz RM, Pan Y, Je HS, Roberts AC, Kim CJ, Berrios J, Colvin JS, Bousquet-Moore D, Lorenzo I, Wu G, Weinberg RJ, Ehlers MD, Philpot BD, Beaudet AL, Wetsel WC, Jiang Y-H. 2011. Synaptic dysfunction and abnormal behaviors in mice lacking major isoforms of Shank3. Human Molecular Genetics 20: 3093–108

Wang X, Yang Y, Zhou Q. 2007. Independent expression of synaptic and morphological plasticity associated with long-term depression. The Journal of Neuroscience 27: 12419–29

Washbourne P, Bennett JE, McAllister AK. 2002. Rapid recruitment of NMDA receptor transport packets to nascent synapses. Nature Neuroscience 5: 751–9

Welch JM, Lu J, Rodriguiz RM, Trotta NC, Peca J, Ding J-D, Feliciano C, Chen M, Adams JP, Luo J, Dudek SM, Weinberg RJ, Calakos N, Wetsel WC, Feng G. 2007. Cortico-striatal synaptic defects and OCD-like behaviours in Sapap3-mutant mice. Nature 448: 894–900

Wendholt D, Spilker C, Schmitt A, Dolnik A, Smalla K-H, Proepper C, Bockmann J, Sobue K, Gundelfinger ED, Kreutz MR, Boeckers TM. 2006. ProSAP-interacting protein 1 (ProSAPiP1), a novel protein of the postsynaptic density that links the spine-associated Rap-Gap (SPAR) to the scaffolding protein ProSAP2/Shank3. The Journal of Biological Chemistry 281: 13805–16

Wenthold RJ, Petralia RS, Blahos J II, Niedzielski AS. 1996. Evidence for multiple AMPA receptor complexes in hippocampal CA1/CA2 neurons. Journal of Neuroscience 16: 1982–9

Won H, Lee H-R, Gee HY, Mah W, Kim J-I, Lee J, Ha S, Chung C, Jung ES, Cho YS, Park S-G, Lee J-S, Lee K, Kim D, Bae YC, Kaang B-K, Lee MG, Kim E. 2012. Autistic-like social behaviour in Shank2-mutant mice improved by restoring NMDA receptor function. Nature 486: 261–265

Wu G-Y, Malinow R, Cline HT. 1996. Maturation of a Central Glutamatergic Synapse. Science 274: 972–976

Yang M, Bozdagi O, Scattoni ML, Wöhr M, Roullet FI, Katz AM, Abrams DN, Kalikhman D, Simon H, Woldeyohannes L, Zhang JY, Harris MJ, Saxena R, Silverman JL, Buxbaum JD, Crawley JN. 2012. Reduced excitatory neurotransmission and mild autism-relevant phenotypes in adolescent Shank3 null mutant mice. The Journal of Neuroscience 32: 6525–41

Yang G, Pan F, Gan W-B. 2009. Stably maintained dendritic spines are associated with lifelong memories. Nature 462: 920–924

Yang Y, Wang X-B, Frerking M, Zhou Q. 2008. Delivery of AMPA receptors to perisynaptic sites precedes the full expression of long-term potentiation. Proceedings of the National Academy of Sciences of the United States of America 105: 11388–93

Yao I, Hata Y, Hirao K, Deguchi M, Ide N, Takeuchi M, Takai Y. 1999. Synamon, a novel neuronal protein interacting with synapse-associated protein 90/postsynaptic density-95-associated protein. The Journal of Biological Chemistry 274: 27463–6

Yasuda H, Barth AL, Stellwagen D, Malenka RC. 2003. A developmental switch in the signaling cascades for LTP induction. Nature Neuroscience 6: 15–6

Yudowski GA, Puthenveedu MA, Leonoudakis D, Panicker S, Thorn KS, Beattie EC, Zastrow M von. 2007. Real-time imaging of discrete exocytic events mediating surface delivery of AMPA receptors. The Journal of Neuroscience 27: 11112–21

Yuste R, Bonhoeffer T. 2004. Genesis of dendritic spines: insights from ultrastructural and imaging studies. Nature reviews. Neuroscience 5: 24–34

Zamanillo D, Sprengel R, Hvalby Ø, Jensen V, Burnashev N, Rozov A, Kaiser KMM, Köster HJ, Borchardt T, Worley P, Lübke J, Frotscher M, Kelly PH, Sommer B, Andersen P, Seeburg PH, Sakmann B. 1999. Importance of AMPA Receptors for Hippocampal Synaptic Plasticity But Not for Spatial Learning. Science 284: 1805–1811

Zhai RG, Vardinon-Friedman H, Cases-Langhoff C, Becker B, Gundelfinger ED, Ziv NE, Garner CC. 2001. Assembling the Presynaptic Active Zone: A Characterization of an Active Zone Precursor Vesicle. Neuron 29: 131–143

Zhang H, Maximov A, Fu Y, Xu F, Tang T-S, Tkatch T, Surmeier DJ, Bezprozvanny I. 2005. Association of CaV1.3 L-type calcium channels with Shank. The Journal of Neuroscience 25: 1037–49

Zhou Q, Homma KJ, Poo M. 2004. Shrinkage of dendritic spines associated with long-term depression of hippocampal synapses. Neuron 44: 749–57

Ziff EB. 1997. Enlightening the Postsynaptic Density. Neuron 19: 1163–1174

Zito K, Scheuss V. 2009. NMDA Receptor Function and Physiological Modulation In L. R. Squire, ed. Encyclopedia of Neuroscience Oxford: Academic Press, p. 1157–1164.

Zitzer H, Hönck HH, Bächner D, Richter D, Kreienkamp HJ. 1999. Somatostatin receptor interacting protein defines a novel family of multidomain proteins present in human and rodent brain. The Journal of Biological Chemistry 274: 32997–3001

Ziv NE, Smith SJ. 1996. Evidence for a role of dendritic filopodia in synaptogenesis and spine formation. Neuron 17: 91–102

6 Appendix

6.1 Glossary

cAMP: cyclic adenosine monophosphate. Second messenger for intracellular signal transduction.

CREB: → cAMP response element-binding protein. Cellular transcription factor. Regulates the expression of c-fos, BDNF (brain-derived neurotrophic factor), tyrosine hydroxylase, neuropeptides, among others. Well documented role in neuronal plasticity and long-term memory formation in the brain.

DAG: diacylglycerol. Produced by → PLC. Membrane-bound second messenger that activates → PKC.

$G_{\alpha q}$: subunit of heterotrimeric → G-Proteins activating → PLC (Figure 19). Coupled to → GPCRs like 5-HT_2, adrenergic α1, and group I metabotropic glutamate receptors (→ mGluR).

G-protein: Guanine nucleotide-binding protein. Classical G-proteins are heterotrimers of one α, one β, and one γ subunit. → GTP binding to the α subunit triggers signalling pathways dependent on subunit type ($G_{\alpha s}$, $G_{\alpha i/o}$, → $G_{\alpha q/11}$). Monomeric G-proteins are commonly referred to as small → GTPases.

GAP: GTPase activating proteins. GAPs can bind to activated small → GTPases and stimulate their GTPase activity, thus terminating the signalling event.

GDP: guanosine diphosphate

GEF: Guanine nucleotide exchange factor. GEFs activate small G-Proteins by stimulating the release of → GDP to allow binding of → GTP. GEFs can be activated by phosphorylation or second messengers like cAMP and Ca^{2+}.

GPCR: G-protein coupled receptors, large family of transmembrane receptors. When activated by their ligand, GPCRs act as → GEFs and activate an associated heterotrimeric → G-protein.

GTP: guanosine triphosphate

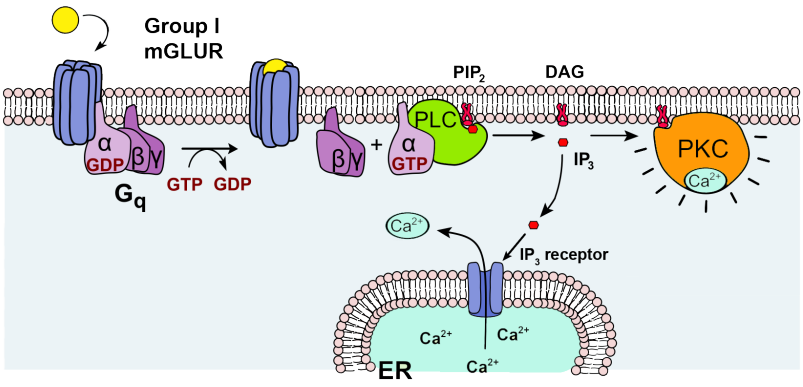

Figure 19: $G_{\alpha q}$ signalling by mGluRs

Group I mGluRs trigger Ca^{2+} release from the ER and activation of → PKC via → PLC signalling. Modified from <http://commons.wikimedia.org/wiki/File:Activation_protein_kinase_C.svg>.

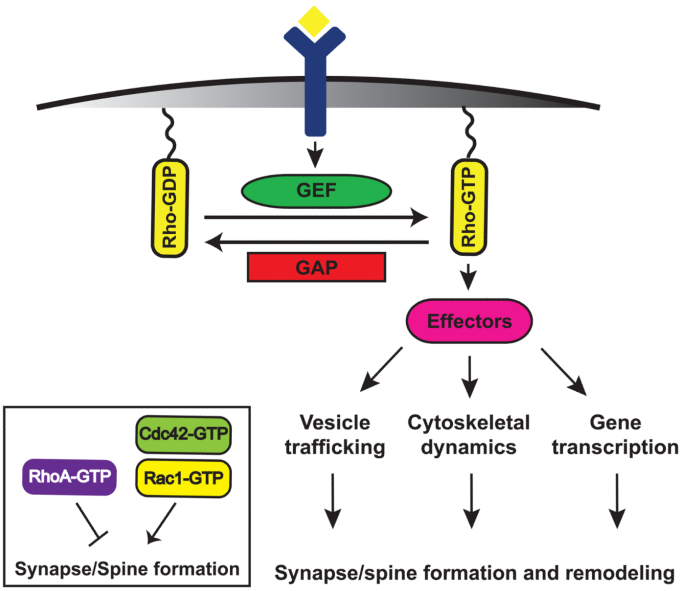

Figure 20: Rho GTPase signalling at synapses

Rho GTPases are small GTPases, their activity is regulated by GEFs and GAPs. Active Rho GTPases regulate a variety of cellular processes via downstream effectors, which ultimately modulate spine morphogenesis and excitatory synapse development. Inset: The Rho GTPase family members have different functions: Rac and Cdc42 promote the formation and growth of synapses and spines; RhoA inhibits synapse development. Modified from Tolias et al. 2011.

GTPase, small: Monomeric G-Proteins with a cytosolic location that are homologues of the α subunit of heterotrimeric → G-proteins. Small GTPases function independent of other subunits and are regulated by → GAPs and → GEFs. They act as molecular switches, active in their GTP-bound, inactive in their GDP-bound form.

IP_3: inositol 1,4,5-triphosphate, produced by → PLC , diffusable second messenger that triggers Ca^{2+} release from intracellular stores via the gating of IP_3 receptors

mGluR: metabotropic glutamate receptors (group I-III) are → GPCRs. Group I receptors comprise mGluR1 and mGluR5 and couple to the G_{aq} subunit. Downstream effects are Ca^{2+} release from the ER via → IP_3 receptors and activation of → PKC (Figure 5.1).

PIP_2: phosphatidylinositol 4,5-bisphosphate, phospholipid component of cell membranes, substrate for hydrolysis by → PLC.

PKC: protein kinase C. Activation in neurons increases the Ser880 phosphorylation of GluA2 subunits, with implications for AMPAR trafficking and clustering.

PLC: phospholipase C. Membrane-bound enzyme that cleaves → PIP_2 into → DAG and → IP_3 when activated by the → G_{aq} subunit of → GPCRs or other (minor) activators.

Rho GTPase: A family of small → GTPases with a role in the development and the structural plasticity of dendrites and spines (Figure 20). RhoGTPases regulate the actin and microtubule cytoskeleton. Prominent family members are RhoA, Rac1, and Cdc42.

6.2 Publication and Statement of Contribution

Schmeisser M*, Ey E*, Wegener S*, Bockmann J, Stempel AV, Kuebler A, Janssen A-L, Udvardi PT, Shiban E, Spilker C, Balschun D, Skryabin B V., Dieck S tom, Smalla K-H, Montag D, Leblond CS, Faure P, Torquet N, Sourd A-M Le, Toro R, Grabrucker AM, Shoichet SA, Schmitz D, Kreutz MR, Bourgeron T, Gundelfinger ED, Boeckers TM. 2012. Autistic-like behaviours and hyperactivity in mice lacking ProSAP1/Shank2. Nature 486: 256–60

* These authors contributed equally to this work.

Some of the experiments described in this thesis result from the collaborative scientific project cited above. In the following I state the contribution of other people to the data presented:

A. Vanessa Stempel

- helped to record the fEPSP input-output curves in P70 animals (Figure 8b)
- helped to record mEPSCs, mIPSCs, and sIPSCs and analysed the data (Figure 9, 10)
- contributed to the recording of CA1 firing thresholds and analysed the data (Figure 11a)
- contributed to the recording of CA1 fEPSP long-term potentiation (Figure 12a)
- contributed to the recordings of A/N ratios at elevated calcium and magnesium concentrations (see methods) (Figure 13)

6.3 Acknowledgements

I performed the experimental work for this PhD thesis in the laboratory of Prof. Dr. Dietmar Schmitz, whom I cannot thank enough for his constant support, trust, patience, and kindness. The security and freedom he provided me with during my time in his lab made working with him a very pleasant experience. I am also grateful for his lucky hand in picking my projects and his wise recommendations for project priorities. In this context I also want to express my thankfulness to Prof. Dr. Stephan Sigrist, who actively involved me into another successful project during my PhD time and who kindly agreed to be the supervisor of this thesis. Lastly, but of great importance, I am deeply thankful for Dietmars hand in choosing great people and his efforts to set up a lab in which it is a pleasure to work in: Thank you, Schmitzlab people (present and past), for always being friendly, warm, helpful, and supportive and for making this group a second home. I will miss you! A special thank you goes to Vanessa Stempel, who pulled me through this project when I was much in need for that: Thank you for your help, your enthusiasm and your interest in (my) scientific problems. I am also grateful to Susanne Rieckmann for her superb management of the knockout animal care and for her never-tiring efforts in setting up the IUE. I also want to thank Sarah Shoichet and Anke Schönherr, who invested quite some time into other parts of the Shank project that did not go into this thesis in the end. Jakob Gutzmann, Jörg Breustedt, Vanessa Stempel, Christian Wozny, Friedrich Johenning, and Dietmar Schmitz significantly improved this thesis with constructive criticism, thank you so much for your help and your time. I furthermore thank the DFG Graduiertenkolleg 1123 „Learning and Memory Consolidation in the Hippocampal Formation“ for its generous financial support and the opportunity to meet a lot of great fellow PhD students.